Author Manuscript

Author Manuscript

Author Manuscript

Author Manuscript

HHS Public Access

Author manuscript

Exp Neurol. Author manuscript; available in PMC 2019 November 01.

Published in final edited form as:

Exp Neurol. 2018 November ; 309: 119–133. doi:10.1016/j.expneurol.2018.07.015.

Evidence of axon connectivity across a spinal cord transection in rats treated with epidural stimulation and motor training combined with olfactory ensheathing cell transplantation.

Michael A. Thornton[1], **Manan D. Mehta**[1], **Tyler T. Morad**[1], **Kaitlin L. Ingraham**[1,2], **Rana R Khankan**[1,2], **Khris G Griffis**[1,2], **Anthony K. Yeung**[1], **Hui Zhong**[1], **Roland R. Roy**[1,3], **V. Reggie Edgerton**[1,2,3], and **Patricia E. Phelps**[1,2,3]

[1]Department of Integrative Biology and Physiology, UCLA, Los Angeles, CA 90095

[2]Molecular, Cellular and Integrative Physiology Interdepartmental Ph.D. Program, UCLA, Los Angeles, CA 90095

[3]Brain Research Institute, UCLA, Los Angeles, CA 90095

Abstract

Olfactory ensheathing cells (OECs) are unique glia that support axon outgrowth in the olfactory system, and when used as cellular therapy after spinal cord injury, improve recovery and axon regeneration. Here we assessed the effects of combining OEC transplantation with another promising therapy, epidural electrical stimulation during a rehabilitative motor task. Sprague-Dawley rats received a mid-thoracic transection and transplantation of OECs or fibroblasts (FBs) followed by lumbar stimulation while climbing an inclined grid. We injected pseudorabies virus (PRV) into hindlimb muscles 7 months post-injury to assess connectivity across the transection. Analyses showed that the number of serotonergic (5-HT) axons that crossed the rostral scar border and the area of neurofilament-positive axons in the injury site were both greater in OEC- than FB-treated rats. We detected PRV-labeled cells rostral to the transection and remarkable evidence of 5-HT and PRV axons crossing the injury site in 1 OEC- and 1 FB-treated rat. The axons that crossed suggested either axon regeneration (OEC) or small areas of probable tissue sparing (FB). Most PRV-labeled thoracic neurons were detected in laminae VII or X, and ~25% expressed Chx10, a marker for V2a interneurons. These findings suggest potential regeneration or sparing of circuits that connect thoracic interneurons to lumbar somatic motor neurons. Despite evidence of axonal connectivity, no behavioral changes were detected in this small-scale study. Together these data suggest that when supplemented with epidural stimulation and climbing, OEC transplantation can increase axonal growth across the injury site and may promote recovery of propriospinal circuitry.

Please address correspondence to: Dr. Patricia E. Phelps, Ph.D., UCLA, Dept. of Integrative Biology and Physiology, Terasaki Life Sciences Building, 610 Charles Young Dr. East, Los Angeles, CA 90095-7239, Telephone: (310) 825-7264 Fax: (310) 206-9184, pphelps@physci.ucla.edu.

Publisher's Disclaimer: This is a PDF file of an unedited manuscript that has been accepted for publication. As a service to our customers we are providing this early version of the manuscript. The manuscript will undergo copyediting, typesetting, and review of the resulting proof before it is published in its final citable form. Please note that during the production process errors may be discovered which could affect the content, and all legal disclaimers that apply to the journal pertain.

Conflict of Interest

V.R.E holds shareholder interest in NeuroRecovery Technologies and holds certain inventorship rights on intellectual property licensed by the Regents of the University of California to NeuroRecovery Technologies and its subsidiaries.

Author Manuscript Author Manuscript Author Manuscript Author Manuscript

Keywords

OECs; climb training; pseudorabies virus; V2a interneurons; somatic motor neurons; sympathetic preganglionic neurons

INTRODUCTION

A severe spinal cord injury (SCI) results in the loss of motor and sensory function below the level of the lesion. Several experimental treatments show therapeutic promise both individually and when combined with complimentary interventions. Olfactory ensheathing cells (OECs), for example, can facilitate moderate locomotor recovery when transplanted into the injured rat spinal cord (Li *et al.*, 1997; Ramón-Cueto *et al.*, 1998; Ramón-Cueto *et al.*, 2000; Plant *et al.*, 2003; López-Vales *et al.*, 2007; Takeoka *et al.*, 2011; Watzlawick *et al.*, 2016) and autologous olfactory bulb-derived OEC transplantation combined with a peripheral nerve graft was associated with functional recovery in a clinically complete SCI patient (Tabakow *et al.*, 2014). OEC-induced changes at the injury site that may promote recovery include reduction of tissue damage, modification of the astrocytic glial scar, and formation of cellular tracts that associate with astrocytes and regenerating axons (Lakatos *et al.*, 2003; Li *et al.*, 2005; Khankan *et al.*, 2016). Consistent with these *in vivo* findings, *in vitro* studies reported that olfactory bulb-derived OECs secrete growth-promoting factors (Woodhall *et al.*, 2001; Lipson *et al.*, 2003), interact favorably with astrocytes (Lakatos *et al.*, 2000; Fairless *et al.*, 2005), and increase neurite outgrowth and sprouting (Chung *et al.*, 2004; Runyan & Phelps, 2009; Khankan *et al.*, 2015).

Lumbosacral epidural stimulation is another promising therapy that can restore locomotor and autonomic function in both rodents and humans with SCI (Gerasimenko *et al.*, 2007; Harkema *et al.*, 2011; Gad *et al.*, 2013; 2015; Rejc *et al.*, 2015). The combination of epidural stimulation with treadmill training generates consistent, weight-bearing locomotion in completely transected rats as early as two weeks after injury (Ichiyama *et al.*, 2005; Lavrov *et al.*, 2006; Gerasimenko *et al.*, 2007; Lavrov *et al.*, 2008). As neural activity is essential for neuronal survival and axon outgrowth during development (Mennerick & Zorumski, 2000), evidence suggests that stimulation-induced activity also enhances neuronal survival, axon growth, and synaptogenesis after injury (Al-Majed *et al.*, 2000; Mondello *et al.*, 2014). Additionally, long-term intraspinal microstimulation of the cervical spinal cord induced significant improvements in forelimb reaching function after a contusion injury (Kasten *et al.*, 2013). These data suggest that spinal cord stimulation can have lasting effects on the locomotor circuitry, and when combined with activity-specific training, may promote long-term functional recovery.

While epidural stimulation with training alone promotes some recovery without axon regeneration, in this study we asked if OEC transplantation, combined with long-term epidural stimulation and climbing, would have additive effects on measures of spared tissue, astroglial bridge formation, and axon regeneration. Because many cell types may confer therapeutic benefits when transplanted after SCI compared to a media or saline-injected control (Tetzlaff *et al.*, 2011), we chose to use dermal fibroblast (FB) transplants as cellular

Author Manuscript Author Manuscript Author Manuscript Author Manuscript

controls. To evaluate axon regeneration in the injury site we used novel anatomical assessments for a severe spinal cord transection model such as the transsynaptic, retrograde tracer pseudorabies virus (PRV) to evaluate synaptic connectivity between the rostral and caudal stumps, and a 3-D visualization of descending motor-associated serotonergic axons in the injury site. We then characterized PRV-labeled interneurons located rostral to the injury site to identify populations of thoracic interneurons that reformed synaptic connections with caudal hindlimb circuits.

MATERIALS AND METHODS

Animals.

The Chancellor's Animal Research Committee at UCLA approved all experiments. Rats were housed under standard conditions with free access to food and water. Olfactory bulb-derived OECs and skin FBs were obtained from 8–10 week old female enhanced green fluorescent protein (eGFP)-expressing Sprague-Dawley rats (Perry *et al.*, 1999). One GFP-expressing rat was used to generate the OECs or FBs transplanted into each spinal rat. An overdose of ketamine-xylazine was used for euthanasia before the extraction of olfactory bulbs and abdominal skin biopsies. Ten female Sprague-Dawley rats (Charles River, 10–12 weeks old) received complete midthoracic spinal cord transections and were maintained for 6–7 mos.

Olfactory bulb-derived OEC and FB cultures.

Methods to prepare OEC primary and immunopurified cultures were similar to those of Ramón-Cueto *et al.* (2000) and identical to the description in Khankan *et al.* (2016). OECs were dissected from the first two layers of GFP-expressing rat olfactory bulbs. Following cell dissociation, OECs were maintained *in vitro* for 5 d and immunopurified using anti-p75-nerve growth factor receptor antibody (1:5; clone 192). Purified OECs were cultured for an additional 7 d before transplantation. Rats were shaved and skin biopsies from the abdominal wall were dissociated into FB cultures as described (Takashima, 2001; Khankan *et al.*, 2016). FBs were passaged 1–2 times before transplantation (12–14 d *in vitro*).

Implantation of stimulating electrodes and intramuscular recording electrodes.

Rats were deeply anesthetized with 1–2.5% isoflurane gas during all surgeries. A midline longitudinal incision was made in the scalp and two stainless steel screws were inserted through pilot holes so that the tip of the screws contacted the cortical dura mater. Teflon-coated wire electrodes (AS632, Cooner Wire) were attached to a head-plug connector (Amphenol) and the head-plug was secured to the skull as described in Iyer *et al.* (2010). Next, partial laminectomies were performed at spinal levels L2 and S1 and the epidural stimulating electrodes were fixed to the dorsal dura mater and attached to the head-plug (Ichiyama *et al.*, 2005). Surgical EMG implantation methods were similar to those in Roy *et al.* (1992) and Gad *et al.* (2013). The skin and fascial incisions exposed the bellies of the soleus and tibialis anterior (TA) muscles bilaterally. Two wires from the head-plug connector were routed underneath the skin from the cranium to each muscle. The electrodes were positioned in the mid-belly of the muscle and secured with two sutures. Proper electrode positioning was verified by muscle contractions elicited by stimulation and then a ground

Author Manuscript Author Manuscript Author Manuscript Author Manuscript

wire was placed subcutaneously in the dorsum of the rat. The skin was sutured and disinfected with betadine, pain medication and fluids were administered, and the rats recovered in an incubator.

Spinal cord injury and cell transplantation.

In a second surgery 3 wks later, a skin incision was made at vertebral levels T6 to L1, the paravertebral muscles were retracted, and partial laminectomies were performed at T7 and T8. The dorsal dura was incised longitudinally and then laterally at both ends to expose the spinal cord. The spinal cord was completely transected near spinal level T7/T8 with micro-scissors, leaving the ventral and lateral dura mostly intact. The rostral and caudal stumps were separated, lifted, and the intact dura was scraped with a glass probe and small cotton balls to sever any spared axons.

Before transplantation, OECs or FBs were rinsed, centrifuged, and re-suspended at a concentration of 100,000 cells per 1 μl in serum-free DMEM (Khankan *et al.*, 2016). Immediately after the transection, ~400,00 total OECs (n = 5) or FBs (n = 5) were injected stereotactically into the spinal cord 1 mm rostral and caudal to the transection as in Ramón-Cueto *et al.* (2000). The spinous processes of the T7–T13 vertebra were stabilized with a stainless steel bar to protect the transection site. Bladder expressions were performed 3×/d for the first mo, and 2×/d at 12-hr intervals thereafter. Rats were inspected daily for weight loss or dehydration and their urine was tested weekly with Multistix 10 SG reagent strips (Siemens). Investigators were blinded to the cell treatment groups from the time of transplantation until completion of the study.

Epidural stimulation, climb training, and behavioral analyses.

Before surgery, rats were trained to climb a 1-inch grid positioned at 60 and 90-degree angles from the horizontal plane (Ramón-Cueto *et al.*, 2000; Ziegler *et al.*, 2011). The inclined grid was connected to a 36-inch tower attached to a low-friction Plexiglas platform covered on 3 sides with dark plastic. Rats received a food reward when they completed the climb and lifted themselves onto the slippery platform. Climb training was conducted for 20 min/d, 3×/wk, for 6 mos, starting 1 mo after spinal cord transection. Rats received 40 Hz epidural stimulation during each climbing session at a voltage of 95% of threshold, which was calculated daily by determining the minimum stimulation to elicit a palpable muscle contraction. Climbing tests were videotaped and EMG activity in the soleus and TA muscles was recorded pre-injury, and with and without epidural stimulation at 3, 5, and 7 mos post-injury.

Two independent observers reviewed the videos of the climbing tests for evidence of hindlimb function. The number of “pushoffs” was counted for each test as described in Ziegler *et al.* (2011). A pushoff was determined visually as hindpaw placement on a horizontal grid rung with ankle joint extension while the paw was lifted and placed onto a higher rung. The number of pushoffs was compared between OEC and FB groups, with and without epidural stimulation, and over time. The corresponding EMG data for each pushoff was examined and the mean and peak amplitudes of the muscle activity for the TA and

Author Manuscript Author Manuscript Author Manuscript Author Manuscript

soleus were averaged and compared. EMG recordings were normalized to recordings made while the rat was inactive.

PRV injections.

At 6 (2 rats) or 7 mos (8 rats) post-transection, pairs of OEC-(n=5) and FB-treated rats (n=5) received injections of eGFP-expressing PRV Bartha-152 (1.21×10^9pfu/mL, generous gift from Drs. Patrick Card and Lynn Enquist, Center for Neuroanatomy of Neurotropic Viruses) into two hindlimb muscles (soleus and/or TA) per rat (Card & Enquist, 2014). Pairs of OEC- and FB-treated rats received PRV injections into the same muscles for comparison. Rats were anesthetized in a BSL-2 biosafety cabinet and an incision was made to expose the target muscle. The soleus received 4 injections of 2.5 μl of virus (10 μl total), while the TA received 8 injections of 2.5 μl of virus (20 μl total). A stainless steel 30-gauge beveled needle attached to a 10 μl Hamilton syringe was used to inject PRV near the motor end plates. The needle was left *in situ* after each injection for ~2 min to prevent backflow. Spinal rats were perfused 6 days after PRV injection.

Tissue preparation.

Rats were anesthetized with ketamine (90 mg/kg) and xylazine (10 mg/kg) intraperitoneally, perfused intracardially with periodate-lysine-4% paraformaldehyde (4% PLP), and post-fixed in 4% PLP for 2–3 hrs (Card & Enquist, 2014). Spinal cords were dissected, placed in 30% sucrose for 48–72 hrs, blocked, embedded in OCT (Tissue-Tek), and stored at −80° C. Sagittal sections (25 μm) were cut and mounted on a series of 16 slides so that each slide represented 6–7 sections 400 μm apart throughout the spinal cord width. Slides were matched between rats so that a comparable sample of the spinal cord width was analyzed for each immunohistochemical experiment.

Immunohistochemistry.

To analyze the injury site, at least one slide containing every 16th section was processed for immunofluorescence with primary antibodies against GFP (1:1000, chicken, Aves Labs Inc., Cat# GFP-1020) and glial fibrillary acidic protein (GFAP, 1:1000, mouse, BD Biosciences, # 556327; 1:10K, rabbit, Dako, # Z0334). An additional marker was used to identify one of the following components: serotonergic axons (5-HT, 1:5000, goat, Immunostar, # 20079), fibronectin (FN, 1:1000, rabbit, Dako, # A0245), neurofilament (NF-200, 1:1000, rabbit, Millipore, # AB1989), and/or aquaporin-4 (Aq4, 1:1000, rabbit, Sigma-Aldrich. # A5971). Slides were rinsed with 0.1M Tris buffer containing 1.4% NaCl and 0.1% BSA, permeabilized, and blocked (normal donkey serum, Jackson ImmunoResearch Laboratories, #017-000-121; normal goat serum, Vector Laboratories, #S-1000) for 1.5 hrs before 24 hr primary antibody incubation. Sections then were incubated with species-appropriate AlexaFluor 488, 555, 594, or 647 secondary antibodies (1:100-500; Jackson ImmunoResearch Laboratories, donkey-anti-chick-488, # 703-545-155; donkey-anti-goat-594, # 705-585-147; donkey-anti-goat-647, # 705-605-147; donkey-anti-rabbit-647, # 711-605-152; donkey-anti-mouse-647, # 715-605-150; Life Technologies: donkey-anti-mouse-555, # A31570; donkey-anti-rabbit-555, # A31572) and counterstained with bis-benzimide (1:500, Sigma-Aldrich, # B2261).

Author Manuscript Author Manuscript Author Manuscript Author Manuscript

To analyze the number and location of the PRVeGFP-labeled neurons rostral to the injury site, four slides from the rostral thoracic (T3–T6) block were processed with chick anti-GFP (1:2000). Slides were matched between rats so that a comparable sample of the spinal cord width was analyzed for all immunohistochemistry analyses. Slides were rinsed with 0.1M phosphate buffer containing 0.9% NaCl and blocked with donkey serum and an avidin-biotin-complex blocking kit (1:1, Vector, # SP-2001) for 1 hr before the primary antibody incubation. The following day, sections were incubated with biotinylated secondary antibody (1:750, donkey-anti-chicken, Jackson ImmunoResearch Laboratories, # 703-065-155), avidin-biotin-complex (1:200) for 1 hr, and visualized with 3–3' diaminobenzidine intensified with 0.02% imidazole.

To identify the PRVeGFP-labeled cells rostral to the injury site, one slide (6–7 sections each) from both the injury site block (T7–T9) and the rostral thoracic block (T3–T6) were processed to evaluate the extent of co-localization with cholinergic neurons (anti-ChAT, 1:500, goat, Millipore, AB144P) or V2a interneurons (anti-Chx10, 1:500, goat, Santa Cruz, # sc-21690) using tyramide signal amplification (TSA-Plus, PerkinElmer, # NEL741). Slide-mounted sections were rinsed with 0.1M Tris buffer containing 1.4% NaCl and 0.05% Tween-20, incubated with TNB, and avidin-biotin-complex blocking solutions (1:1), and then incubated with the primary antibody for 48–72 hours at 4°C. We used the appropriate biotinylated secondary antibodies (1:250–500, Jackson ImmunoResearch Laboratories, donkey-anti-chicken, # 703-065-155; Vector, horse-anti-goat, # BA-9500), streptavidin horseradish peroxidase (1:250–500, PerkinElmer, # FP1047), and cyanine-3 fluorophore diluted in amplification buffer (1:250, PerkinElmer, # FP1135).

Image acquisition and analyses.

Panoramic micrographs were obtained with an Olympus AX70 microscope equipped with an AxioCam HRcRv.2 and ZEN software (2012, Zeiss). Confocal images were taken with a Zeiss LSM 510/800 microscope. All cell counts and contour area tracing analyses were conducted with Neurolucida and Neurolucida Explorer (v10, MicroBrightField). Images were pseudocolored, edited, and compiled into figures with Adobe Photoshop and Illustrator.

To determine the lesion core volume and percent spared tissue, one slide was labeled for GFAP and Aq4 to identify astrocyte intermediate filaments and processes and fibronectin (FN) to mark the extracellular matrix in the lesion core. Total cord volume, lesion core volume, and cyst volume were calculated as described (Kubasak *et al.*, 2008). The spared tissue volume was expressed as a percentage of the total cord volume for each rat. To quantify the area of astrocytes and axons in the injury site we used the Neurolucida contours function to measure the GFAP-positive extensions, 5-HT-positive axons, and neurofilament-labeled axons. To quantify the extent of 5-HT axon regeneration we measured the area of 5-HT immunoreactivity in the injury site and counted 5-HT-positive axon bundles that crossed the rostral glial scar border, as described (Khankan *et al.*, 2016). Axons labeled with neurofilament were traced as reported for the 5-HT axons, but axons that originated from peripheral roots were excluded.

PRVeGFP-labeled cells were counted if a distinct cell soma and at least one process were identified. Cell counts were normalized to the section area (cm^2). For the cell location

Author Manuscript Author Manuscript Author Manuscript Author Manuscript

analyses, PRVeGFP-labeled cells within laminae I-V were designated as dorsal, laminae VII, X, and the intermediolateral (IML) cell column as intermediate, and laminae VIII and IX as ventral spinal cord. In preliminary experiments most PRVeGFP-positive, NeuN-negative cell bodies were less than 10 μm in diameter, and therefore we used a 10 μm cutoff when counting PRV-eGFP-positive cells to exclude infected astrocytes that do not possess the molecular machinery to facilitate viral spread (Card *et al.*, 1993). To analyze the phenotype of PRV-labeled thoracic interneurons, one slide from the T3–T6 region and another from the injury site block (T6–T7/8) were processed to assess co-localization with choline acetyltransferase (ChAT) and the transcription factor Chx10. Any cells that appeared co-localized in the panoramic photomicrograph were reimaged with confocal microscopy.

We only considered that PRVeGFP-labeled cells rostral to the transection could be connected to somatic motor neurons if the transected rats had 1) evidence of axons (5-HT-, NF-, and PRV-labeled) crossing the injury site, and 2) PRVeGFP double labeling with cell-specific markers in typical locations for somatic interneurons known to participate in locomotor circuits. We focused on two groups of somatic interneurons: cholinergic propriospinal (medial partition and central canal cluster cells) and V2a interneurons. The cholinergic interneurons are found in or near lamina X, form “C-type” synapses with somatic motor neurons, and function in locomotor circuits (Phelps *et al.*, 1984; Phelps et al., 1990; Huang *et al.*, 2000; Miles *et al.*, 2007; Zagoraiou *et al.*, 2009, Jordon et al., 2014). The V2a glutamatergic interneurons express Chx10, and are concentrated in the intermediate spinal cord (Dougherty and Kiehn, 2010; Ni *et al.*, 2014; Ueno *et al.*, 2018). To our knowledge, neither the medial partition cells nor the Chx10 interneurons contact sympathetic preganglionic neurons. Sympathetic interneurons are known to be glutamatergic, GABAergic and glycinergic, and cholinergic, but currently there are no definitive interneuron markers to distinguish SPN-connected circuits (Schramm, 2006; Deuchars, 2015; Ueno *et al.*, 2016).

3-D visualization.

We created a 3-D rendering of the injury site in the OEC-treated spinal rat with marked evidence of regeneration. Twenty-two sagittal sections with an inter-section interval of 100 μm were immunolabeled for astrocytes (GFAP), serotonergic axons and PRVeGFP-labeled neurons. Neurolucida was used to make contour traces of GFAP and 5-HT labeling, and to place markers for PRVeGFP-labeled cells. The contours and markers belonging to a single section were grouped using Neurolucida’s serial section manager and then assigned to the z-value. Sections were overlaid in sequence and aligned to the prior section by matching multiple regions of interest that were consistent across sections (e.g., the meningeal scar). To rebuild axon tracts, the contours associated with the same axon bundle region were manually grouped and saved as different contours. The 3-D visualization feature then was used to construct the model.

Statistical analyses.

Due to the small sample size and possible lack of normality, statistical comparisons for anatomical measures were conducted in R (3.2.2; R Core Team, 2015) using re-sampling techniques (Efron & Tibshirani, 1991). The null hypothesis was simulated 10,000 times

Author Manuscript Author Manuscript Author Manuscript Author Manuscript

using the non-parametric bootstrap approximation to compute non-parametric standard errors and corresponding *p* values. Our experimental effect sizes were compared to the bootstrapped confidence intervals to generate *p*-values.

To assess the association between 5-HT axon area and astrocyte extension area in the injury site, we carried out a linear regression and also reported the corresponding Pearson correlation (*r*). Linear regression was used since the corresponding scatter plot showed a linear relationship. All group comparison plots were exported from JMP (Software Version 10, SAS Institute, Cary, NC) and represent the group mean +/− bootstrapped SEM. Statistical significance was determined at $*p < 0.05$ or $**p < 0.01$.

The behavioral tests means were compared using a parametric repeated measure (mixed) model allowing correlation between multiple measurements on the same animal. Normal quantile plots and the Shapiro-Wilks test confirmed that the errors followed a normal distribution, justifying the use of a parametric model.

RESULTS

Astrocyte bridges spanned the injury site in two OEC- and two FB-treated rats.

After severe SCI, large cysts form around the injury site in both rats and humans and cause further tissue damage and restrict recovery (Byrnes *et al.*, 2010). Previous studies found that OEC-transplantation reduced lesion volume size compared to media-injected controls at 7-mos post-injury (Kubasak *et al.*, 2008; Takeoka *et al.*, 2011). We identified the fibrotic extracellular matrix of the lesion core and the glial scar borders to measure the volume of the lesion and the percent spared tissue within an 8 mm length of spinal cord centered on the injury site (Fig. 1A). The lesion and spared tissue volumes did not differ between OEC- and FB-transplanted rats (data not shown).

We found that six of the ten spinal rats used in the study (OEC #2, OEC #4, OEC #5, FB #2, FB #4, and FB #5) had well defined rostral and caudal glial scar borders and distinct FN-positive separations throughout the injury site (Fig. 1B–C, arrowheads). We also found, however, that the remaining four rats (OEC #1, OEC #3, FB #1, and FB #3) had at least one region in which astrocytes spanned the rostrocaudal length of the injury site (Fig. 1D and E, arrows). These GFAP-immunopositive astrocyte bridges appeared continuous and connected the rostral and caudal stumps. Both of the OEC-treated rats (OEC #1, and OEC #3) had multiple astrocyte bridges throughout the dorso-ventral extent of the spinal cord (Fig. 1D, arrows), whereas the FB-treated rats (FB #1 and FB #3) each had bridges continuous with only their ventral spinal stumps (Fig. 1E, small arrow).

When we examined the injury sites of our spinal rats for evidence of cell transplant survival we found that neither OECs nor FBs survived to 7 mos post-transplantation. OECs are hypothesized, however, to alter the astroglial scar and be more permissive to axon regeneration at early post-transplantation time points even if the cells did not survive the entire course of recovery (Li *et al.*, 2005; Khankan *et al.*, 2016). We decided, therefore, to look further at the relationship between the astroglial scar and axon regeneration.

Author Manuscript Author Manuscript Author Manuscript Author Manuscript

More axons were detected crossing the rostral scar border and within the injury site in OEC- than in FB-transplanted rats.

We examined the amount of surviving axons in the injury sites using the panaxonal marker neurofilament-200 (NF) in OEC- and FB-transplanted rats. In all 10 rats we observed some NF-positive axons in the injury site, but in three rats (OEC #1, OEC #3, and FB #1) there were NF-labeled axon bundles that spanned the width of the lesion between the glial scar borders (Fig. 2A–B, OEC #3, arrowheads denote likely bridges). Confocal imaging of a ventral bridge 400 μm from the section shown in Figure 2A revealed multiple discontinuous NF-labeled axons within the GFAP-negative lesion core (Fig. 2B1–2). We quantified the NF-positive area between the GFAP-positive boundaries and found that OEC-transplanted rats had a mean area of 314,401 ± 54,798 μm^2, while FB-transplanted rats averaged 115,993 ± 32,756 μm^2 at 7-mos post-transection (Fig. 2D, $p = 0.002$). Thus, OEC-transplantation increased the amount of NF-positive axons in the lesion core.

To assess motor-associated axon growth through the glial scar border, we counted the number of descending serotonergic (5-HT-positive) axon bundles that crossed the rostral glial scar border and extended into the injury site (Fig. 2C, arrowheads). OEC-transplanted rats had an average of 58 ± 6 5-HT axon bundles crossing the rostral scar border compared with FB-treated rats that averaged 27 ± 9 axon bundles (Fig. 2E, $p = 0.007$). Together, the NF area and 5-HT axon bundles data suggest that, compared to the FB group, the injury sites of OEC-transplanted rats were more permissive to long-term axonal regrowth and survival.

Axons regenerated through the lesion core on thin astrocyte bridges.

Because substantial functional recovery can occur through the regeneration or sparing of a small number of axons (Keyvan-Fouladi *et al.*, 2003) and astrocytes provide permissive substrates for axon growth into the injury site (Anderson *et al.*, 2016), we asked if CNS axons were associated with astrocyte bridges. Specifically, we assessed the presence of 5-HT-positive axons and GFAP-positive bridges in the lesion cores of OEC- and FB-transplanted rats. Astrocyte extensions were defined as thin GFAP-positive processes that projected more than 500 μm from the glial scar border and were less than 100 μm in width. We found that the mean area of these astrocyte extensions did not differ between the OEC- and FB-transplanted groups (304,540 ± 65,736 μm^2 and 267,567 ± 93,994 μm^2 respectively, Fig. 3A). The mean area of 5-HT immunoreactivity extending beyond the scar border (either with astrocyte extensions or within the GFAP-negative lesion core) also did not differ between OEC (84,720 ± 18,953 μm^2) and FB (55,204 ± 16,820 μm^2) rats (Fig. 3B). When the data of the GFAP- and 5-HT-positive areas were plotted together for each individual rat, however, we observed a positive correlation between the GFAP-immunoreactive astrocyte bridge area and the 5-HT axon area (Fig. 3C, $r = .83$, $p = 0.003$). This correlation indicates that 5-HT axons can potentially regenerate into or at least survive in the lesion site together with astrocytes; this finding is consistent with recent evidence that astroglial scar formation aids in long-term axon regeneration after SCI (Anderson *et al.*, 2016).

We also noticed that two rats in particular, OEC #1 and FB #1 (shown in Fig. 3D–I), had large areas of GFAP and 5-HT immunoreactivity in the injury site compared to the other 8 spinal rats (Fig. 3C, red boxes). Upon closer examination we found that OEC #1 had bundles

Author Manuscript Author Manuscript Author Manuscript Author Manuscript

of 5-HT axons associated with a continuous bridge of astrocytes that extended to the dorsomedial area of the caudal stump (Fig. 3D–E). To better visualize the complicated network of 5-HT axons in this rat, we created a 3-D reconstruction (Fig. 3F) of the GFAP-positive area (blue) and 5-HT-positive axon bundles (red) from sagittal sections at 100 μm intervals within 2–3 segments of the injury site. An enlargement of the injury site revealed that descending 5-HT axons that reached the caudal stump (Fig. 3F, arrowheads) were broadly distributed within the central part of the injury site. Due to the highly disorganized appearance of the 5-HT axons along dorsomedially-located bridges, these areas may represent axon regeneration. A video of the 3-D reconstruction for OEC #1 is shown in Supplemental Video 1.

In contrast to the 5-HT-labeled axons in OEC #1, FB #1 had a long, straight bridge composed of 5-HT axons that appeared continuous along the ventral border between the rostral and caudal spinal stumps (Fig. 3G–H, arrowhead). Confocal microscopy revealed that astrocytic processes were closely associated with 5-HT axons that bridged the injury site (Fig. 3I, arrowheads). Due to the location of the bridge in FB #1, it is likely that these long 5-HT axons represent spared or newly sprouted axons, rather than regeneration.

Evidence of an incomplete transection in FB #1 but not in OEC #1.

Of the ten transected rats, only two (OEC #1 and FB #1) had astrocyte bridges that persisted throughout multiple sections (>300 μm in the medio-lateral extent of the spinal cord). Interestingly, these same two rats also had remarkable evidence of axonal connectivity across the injury site, which may be due either to axon regeneration or axon sparing caused by an incomplete transection. To determine the likelihood of an incomplete transection, the spinal cord transection sites of OEC #1 and FB #1 were carefully examined in 18–22 GFAP-labeled sagittal sections spaced at 50–100 μm intervals. Analysis of OEC #1 showed bridges in the dorsal and intermediate, but not in the ventral spinal cord (Fig. 4A and C). Analysis of FB #1, however, revealed a clear ventral bridge that included a substantial area of possible spared tissue (Fig. 4B, D, and E). Due to the transection methods used in this study, it is highly unlikely that axons in the dorsal or intermediate spinal cord would remain intact when the ventral spinal cord was transected, whereas an isolated ventral bridge leaves open the possibility of an incomplete injury. Based on the series of GFAP-labeled sections examined, we suspect that FB #1 had an area of spared tissue. Because the detection of axonal connectivity in a complete transection model is rare, we chose to further analyze this rat as it provides an important comparison for OEC #1.

PRV injections into hindlimb muscles identified lumbar somatic motor neurons.

We injected PRVeGFP into the soleus and/or TA muscles to identify locomotor circuits that were synaptically connected to muscle-specific somatic motor neurons (SMNs, Fig. 5A). We detected PRVeGFP and choline acetyltransferase (ChAT) double labeled SMNs in lamina IX at lumbar levels L3–L6 in 8 of 10 PRV-injected rats (Fig. 5B, arrowheads). Occasional PRVeGFP-positive, ChAT-negative neurons were detected near the lumbar SMNs, and may represent premotor interneurons or SMNs that no longer expressed ChAT after prolonged PRV infection (Fig. 5B–B2, arrow). We also found PRVeGFP- and ChAT-labeled axons in the lumbar ventral roots that illustrate the viral entry route into the spinal cord (Fig. 5C). The

Author Manuscript Author Manuscript Author Manuscript Author Manuscript

two rats without PRV-labeled lumbar SMNs (OEC #4 and FB #5) were excluded from subsequent analyses.

PRV-labeled axons were detected in the injury sites of OEC #1 and FB #1.

To assess axonal connectivity we analyzed the transection sites for the presence of PRV-labeled axons (green) and GFAP-positive bridges of astrocytes (blue). In OEC #1 several PRV-labeled axons projected between the rostral and caudal stumps within dorsomedially-located astrocytic bridges (Fig. 6A, B). In FB #1 a PRV-labeled axon traversed the lesion site along a thin glial bridge that likely bordered a large ventral cyst *in vivo* (Fig. 6C, white arrows). High magnification images showed that the PRV-labeled axons bridged the lesion site (Fig. 6D–D2) in an area populated with astrocytes (Fig. 6E, arrowheads).

To evaluate the location of the PRVeGFP-labeled neurons (green spheres) within the injury site of OEC #1, we used the 3-D reconstruction of the spinal cord to visualize their relative distribution (Fig. 6F, F1; dotted lines mark the injury site area). There were 714 PRVeGFP-labeled cells detected within the thoracic segments caudal to the transection (T7/8), 44 cells in the estimated injury site, and 65 cells located in the rostral stump, within the 22 sagittal sections analyzed (spaced 100 μm apart). The substantial evidence of PRV transport across the injury site, combined with the disorganized growth of 5-HT- and NF-labeled axons (Figs. 2, 3) suggests that long-term axonal regeneration may have occurred in OEC #1. Because of the presence of a thin, straight bridge in multiple injury site sections of FB #1 (Figs. 1E, 3G–I, 4B,D,E, 6C–E) we suspect that axon sparing contributed to the connection.

PRV labeling was detected in thoracic neurons rostral to the complete transection.

Next we analyzed the T3–T6 thoracic spinal cord levels rostral to the transection site to further assess transsynaptic viral transport across the lesion (Fig. 7A). In 1 of 4 OEC-transplanted rats (OEC #1) and 2 of 4 FB-transplanted rats (FB #1, and FB #2), PRVeGFP-labeled cells were found rostral to the T7/8 transection (Fig. 7B–D). We evaluated 21–24 sagittal sections (100 μm interval) per rat to assess PRVeGFP-labeled cells in each transplant group. OEC #1 had an average cell density of 14 ± 4 cells/cm^2, whereas FB #1 and FB #2 had averages of 32 ± 8 and 5 ± 2 cells/cm^2, respectively. We mapped the dorsoventral and mediolateral locations of PRVeGFP-labeled cells for each of these three rats in the T3–T6 region (Fig. 7E–G). An average of 16% of the total number of PRVeGFP-labeled cells were in laminae I-V, 78% in laminae VII, X, or the IML, and 6% in laminae VIII or IX (Fig. 7E–G, stacked bar graphs).

Analysis of cell location along the mediolateral axis revealed anatomical differences in the PRV-labeling distributions in the three rats with PRV-labeled cells rostral to the injury (Fig. 7E–G, gradient histograms, the y-axis scale adjusted/rat). While OEC #1 (Fig. 7E) and FB #1 (Fig. 7F) had thoracic PRV-labeling consistent with the side(s) of injection and labeled cells throughout the ipsilateral width of the grey matter, most labeled cells in FB #2 (Fig. 7G) were 500 to 900 μm from the central canal with only a few in lamina X. To better visualize the locations and sizes of the PRVeGFP-labeled cells, we plotted the rostrocaudal and dorsoventral locations of the cells along with their approximate size (long diameter of the cell body, reflected in the size of the data points) on a schematic of the thoracic spinal

Author Manuscript Author Manuscript Author Manuscript Author Manuscript

cord (Fig. 7H). Mean somata diameter was 22 ± 1.30 μm for OEC #1, 27 ± 0.93 μm for FB #1, and 27 ± 3.72 μm for FB #2. Cell body diameters ranged from ~10–50 μm, indicating the presence of multiple neuronal populations.

Because there is sympathetic innervation of blood vessels in hindlimb muscles, injected PRV may be transported through the sympathetic chain ganglia circuits (Rotto-Percelay *et al.*, 1992; Kerman *et al.*, 2003). Based on the sympathetic innervation of the gastrocnemius (Rotto-Percelay *et al.*, 1992), we anticipated that the sympathetic innervation from blood vessels in the TA and soleus would be conveyed to sympathetic preganglionic neurons (SPNs) several segments caudal to the transection, i.e., T11-L2. Yet in all three rats with PRV-labeled cells rostral to the injury site, we found large neurons in a location consistent with a SPN identity. For example, a cluster of large PRV-labeled neurons (cell body diameters of 25–40 μm) was detected in FB #2 near T6 ipsilateral to the PRV infection, and they probably represent SPNs retrogradely labeled via the hindlimb vasculature (Fig. 7H, red box). The cell sizes and locations observed in FB #2, combined with the fact that there was no evidence of axon regeneration or sparing in the injury site (Fig. 1C), suggest that the PRV-labeling in this rat occurred only via the sympathetic chain to SPNs located rostral to the T7/T8 transection. On the other hand, in addition to some SPNs, OEC #1 and FB #1 both have evidence of axon connectivity across the injury site (OEC #1 shown in Figs. 1D, 3D–F, 4A,C, 6B–B2, F–F1; FB#1 shown in Figs. 1E, 3G–I, 4B,D–E, 6C–E) and a PRV thoracic labeling pattern of cells that resemble those of locomotor-related circuits. A percentage of the PRV-labeled thoracic interneurons in these two rats, therefore, appear to be synaptically connected to lumbar somatic circuits.

Multiple populations of thoracic cholinergic neurons were labeled with PRV.

There is evidence that the cholinergic central canal cluster and partition cells are propriospinal systems that modulate locomotion (Phelps *et al.*, 1984; Miles *et al.*, 2007; Jordan *et al.*, 2014; Tillakaratne *et al.*, 2014, Zagoraiou *et al.*, 2009). We analyzed the co-localization of PRVeGFP and ChAT in 1 slide/rat both in the injury site (T6–T8) and the further rostral thoracic (T3–T6) spinal cord to identify cholinergic propriospinal interneurons and SPNs labeled with PRV. In OEC #1, ~12% of PRVeGFP-labeled cells co-localized with ChAT (6/52 cells), and there was a mix of large, lateral cells and smaller interneurons found near the central canal. FB #1 had a similar spatial distribution with ~14% of PRV-labeled cells that co-expressed ChAT (13/93 cells) and a subset of cholinergic interneurons were found in lamina X (Fig. 8A). In contrast, FB #2 had very few PRV-labeled cells and only one large neuron in the IML that co-expressed ChAT (1/6 PRV-labeled cells, Fig. 8B). The medially located cholinergic interneurons labeledin OEC #1 and FB#1, therefore, may represent a propriospinal system labeled with PRV through synaptic connections to caudal locomotor circuits.

V2a interneurons were labeled with PRV rostral to the transection.

To identify a specific locomotor-related propriospinal system we asked if PRVeGFP-labeled neurons co-expressed Chx10, a homeodomain transcription factor that marks V2a glutamatergic interneurons with long-descending axons that innervate SMNs (Al-Mosawie *et al.*, 2007; Ni *et al.*, 2014). Initially, we showed that Chx10 is expressed in both the intact

Author Manuscript Author Manuscript Author Manuscript Author Manuscript

(Fig. 8C) and injured lumbar spinal cord (Fig. 8D–E, OEC #5). Several of the injured rats had many Chx10-positive nuclei co-localized with PRVeGFP (Fig. 8C–E) in the lumbar spinal cord, most of which were located near or in laminae VII or X, but others were within the ventral and deep dorsal horns (Fig. 8C, D).

When we analyzed the segments rostral to the injury site (T3–T7/8) in our transected rats, we found that 12% of PRV-labeled cells in OEC #1 (Fig. 8F; 3/26 cells), 34% in FB #1 (Fig 8G; 40/119 cells), and 0% in FB #2 (0/9 cells) co-expressed Chx10. These data imply that PRV-positive V2a interneurons located rostral to the complete transection reconstituted or sustained connections to locomotor circuits caudal to the injury in the same two rats with evidence of axon projections across the injury site, i.e., OEC #1 and FB #1.

Behavioral recovery did not differ between OEC- and FB-transplanted rats.

To test functional recovery, we examined the performance of the spinal rats on a grid climbing locomotor task at 3, 5, and 7 mos post-injury. Previous studies reported that completely transected OEC-treated rats had a greater number of hindlimb pushoffs from the wire grid and higher EMG amplitudes when performing the grid climbing task compared to media controls (Ziegler *et al.*, 2011). Here we analyzed the number of grid pushoffs determined by visual observation of the coordinated movement of hindpaw placement from one horizontal rung to another higher on the grid. In this study the number of pushoffs did not differ between OEC and FB groups at 3, 5, or 7 mos post-transection, either with or without concurrent epidural stimulation (data not shown). The corresponding mean and peak amplitudes of EMG recordings from the TA and soleus muscles during each pushoff also did not differ between transplant groups (data not shown), possibly because of the limited sample size compared to Ziegler *et al.* (2011). The small sample size in this study is due to our original intention of testing new methods to guide the design of our next larger study.

DISCUSSION

In this study we found that the projection of NF-positive axons and 5-HT axon bundles into the injury site was significantly greater in rats that received an OEC transplantation combined with a 6-month regimen of sub-threshold lumbosacral epidural stimulation and voluntary climb training than those that received a FB transplantation with the same training regimen. Multiple anatomical assessments showed evidence of axon connectivity in two rats, one from each group, including continuous bridges of reactive astrocytes associated with 5-HT- and NF-positive axons across the injury site. Additionally, viral tracing with PRV showed that axons of rostral thoracic interneurons crossed the transection site and made connections with neural circuits that innervated lumbar SMNs in these same two rats. Together, our findings suggest that epidural stimulation with climb training, combined with cell transplantation can facilitate axon regeneration in a long-term rodent model of severe SCI.

Interpretation of regeneration in complete and incomplete transections

The major reason for using a complete transection model, rather than a mild injury, is that it allows for a more definitive identification of axon regeneration. Evidence shows that even a

Author Manuscript Author Manuscript Author Manuscript Author Manuscript

small amount of tissue sparing may allow for motor recovery and provide a surface for spontaneous axon sprouting. It is, therefore, important that stringent criteria are met in order to differentiate between axon regeneration and sparing (Steward *et al.*, 2003). In this study we found two rats with substantial evidence of anatomical connectivity across the injury site, but one of these rats (FB #1) had a small area of spared ventral spinal cord tissue and straight axons that projected directly across the injury site. Our surgical methods used scissors to cut the spinal cord and the stumps were lifted and separated to verify the complete transection. The ventral dura mater, however, remained intact so it is possible that some ventrally located axons adhered to the dura and resulted in an "incomplete" transection. It is nearly impossible, however, for a piece of the dorsal or intermediate spinal cord to remain intact while the ventral side was completely severed, as seen in OEC #1. Due to the multiple axonal bridges with associated astrocytes, plus the highly disorganized 5-HT projections seen in OEC #1 we propose that these connections could be due to regeneration as they meet most of the criteria described by Steward *et al.* (2003). The differences in the anatomical characteristics between these two rats provide an important example between axon sparing and regeneration.

OEC graft survival and lasting effects on the injury site

Several groups have reported the long-term (> 4 months) neuroprotective effects of OEC transplantation (López-Vales *et al.*, 2007; Guest *et al.*, 2008; Takeoka *et al.*, 2011; Ziegler *et al.*, 2011). Recently we learned that OEC and FB transplants die between 4–8 weeks post-injury in our short-term study that used identical transection and transplantation methods as the present study. In Khankan et al. (2016) we reported that even after cell death, OECs had lasting effects that substantially modified the injury site and promoted axon outgrowth. In addition, Li *et al.* (2016) used a unilateral corticospinal tract lesion and found that rats transplanted with OECs continued to display directed forearm reaching after immunosuppression was withdrawn and the transplanted OECs died. While these data are promising, long-term survival of transplanted OECs may allow for even more robust recovery after transection.

PRV transport through locomotor and autonomic circuits

Rotto-Percelay *et al.* (1992) used PRV injections into the medial gastrocnemius of intact and dorsal rhizotomized adult rats to examine the contribution of somatic and autonomic circuits. They reported specific retrograde transsynaptic infection of somatic motor neurons (L1–L6), sympathetic preganglionic neurons (T11-L2), and the associated interneuronal circuits in the thoracolumbar spinal cord. We chose the T7/T8 transection site that was several spinal segments rostral to the reported location of hindlimb sympathetic preganglionic neurons (Rotto-Percelay *et al.*, 1992), yet some large ChAT/PRV-labeled neurons were detected in the IML in three rats rostral to the transection.

Based on the size, location, and phenotype of the PRV-labeled neurons rostral to the transection, together with the analyses of the injury sites, we suspected that one of these rats (FB #2) had PRV transport solely through the sympathetic trunk. The other two rats (OEC #1 and FB #1) also had PRV-labeled axons that crossed within the injury site, and PRV-labeled cell types consistent with somatic locomotor circuitry. Due to the lack of unique

Author Manuscript Author Manuscript Author Manuscript Author Manuscript

autonomic interneuron markers (Schramm, 2006), we were unable to distinguish interneurons associated with the sympathetic circuits. Instead, we focused on identifying locomotor-specific interneuronal populations.

The role of propriospinal V2a interneurons in functional recovery after SCI

Chx10-positive spinal V2a interneurons contribute significantly to coordinated locomotion, provide excitatory input to somatic motor neurons, and are located throughout the rostrocaudal length of the spinal cord (Crone *et al.*, 2008; Dougherty & Kiehn, 2010; Ni *et al.*, 2014). Recent work showed that V2a glutamatergic interneurons are recruited into the functional phrenic network following high cervical injury and can drive phrenic motor neuron firing in the absence of supraspinal input (Cregg *et al.*, 2017; Zholudeva *et al.*, 2017). Additionally, co-tracing, electrophysiological, and chemogenetic silencing techniques showed that motor corticospinal tract neurons project directly to cervical Chx10-positive premotor interneurons and control distinct aspects of the forelimb reaching movement (Ueno *et al.*, 2018). Furthermore, the reorganization of propriospinal interneuronal circuits that cross the injury site and project to lumbar spinal segments may be a key mechanism in the recovery of sensorimotor function after SCI (Bareyre *et al.*, 2004; Courtine *et al.*, 2008). We suggest that the PRV-labeled, Chx10-positive interneurons detected rostral to the injury represent evidence of propriospinal circuits that regenerated synaptic connections across the spinal cord transection site.

Results from this long-term study showed that axonal regeneration in the injury site was associated with the formation of astrocyte bridges. More importantly, we found substantial evidence of PRV-labeled axon regeneration after spinal cord transection. These findings led us to develop stringent criteria to identify descending axonal connections to locomotor circuits innervating hindlimb muscles in order to better assess axon regeneration. While OEC transplantation combined with epidural stimulation and climb training likely affected axonal regeneration to a larger extent than FB transplantation, further study is needed to determine the extent that this combinatorial approach could be developed into a successful treatment for SCI.

Supplementary Material

Refer to Web version on PubMed Central for supplementary material.

ACKNOWLEDGEMENTS

This work was supported by the National Institute of Neurological Disorders and Stroke [1R01NS076976; VRE/PEP], the National Institute of Health Center Grant [P400D010996] and the National Institute of Child Health and Human Development [P30HD004612; IDDRC microscopy core]. We thank Dr. Larry Schramm for helpful discussions about sympathetic preganglionic neurons and PRV labeling, Dr. Patrick Card for advice on the PRV techniques, Dr. Jeff Gornbein for assistance in the statistical analyses, Aly Mulji for the lesion core analyses, Deborah Wang for assistance with Multistix testing, and the many UCLA undergraduate students who helped with animal care.

Author Manuscript Author Manuscript Author Manuscript Author Manuscript

REFERENCES

Al-Majed AA, Brushart TM & Gordon T (2000) Electrical stimulation accelerates and increases expression of BDNF and trkB mRNA in regenerating rat femoral motoneurons. Eur J Neurosci, 12, 4381–4390. [PubMed: 11122348]

Al-Mosawie A, Wilson JM, & Brownstone RM (2007) Heterogeneity of V2-derived interneurons in the adult mouse spinal cord. Eur J Neurosci, 26, 3003–3015. [PubMed: 18028108]

Anderson MA, Burda JE, Ren Y, Ao Y, O'Shea TM, Kawaguchi R, Coppola G, Khakh BS, Deming TJ & Sofroniew MV (2016) Astrocyte scar formation aids central nervous system axon regeneration. Nature, 532, 195–200. [PubMed: 27027288]

Bareyre FM, Kerschensteiner M, Raineteau O, Mettenleiter TC, Weinmann O & Schwab ME (2004) The injured spinal cord spontaneously forms a new intraspinal circuit in adult rats. Nat Neurosci, 7, 269–277. [PubMed: 14966523]

Byrnes KR, Fricke ST & Faden AI (2010) Neuropathological differences between rats and mice after spinal cord injury. J Magn Reson Imaging, 32, 836–846. [PubMed: 20882614]

Card JP & Enquist LW (2014) Transneuronal circuit analysis with pseudorabies viruses, in: Current Protocols in Neuroscience. Wiley, Hoboken, NJ, pp. 1.5.1–1.5.39.

Card JP, Rinaman L, Lynn RB, Lee B-H, Meade RP, Miselis RR, & Enquist LW, (1993) Pseudorabies virus infection of the rat central nervous system: Ultrastructural characterization of viral replication, transport, and pathogenesis. J Neurosci 13, 2515–2539. [PubMed: 8388923]

Chung RS, Woodhouse A, Fung S, Dickson TC, West AK, Vickers JC & Chuah MI (2004) Olfactory ensheathing cells promote neurite sprouting of injured axons in vitro by direct cellular contact and secretion of soluble factors. Cell Mol Life Sci, 61, 1238–1245. [PubMed: 15141309]

Courtine G, Song B, Roy RR, Zhong H, Herrmann JE, Ao Y, Qi J, Edgerton VR & Sofroniew MV (2008) Recovery of supraspinal control of stepping via indirect propriospinal relay connections after spinal cord injury. Nat Med, 14, 69–74. [PubMed: 18157143]

Cregg JM, Chu KA, Hager LE, Maggard RS, Stoltz DR, Edmond M, Alilain WJ, Philippidou P, Landmesser LT, Silver J (2017) A latent propriospinal network can restore diaphragm function after high cervical spinal cord injury. Cell Reports 21, 654–665. [PubMed: 29045834]

Crone SA, Quinlan KA, Zagoraiou L, Droho S, Restrepo CE, Lundfald L, Endo T, Setlak J, Jessell TM, Kiehn O & Sharma K (2008) Genetic ablation of V2a ipsilateral interneurons disrupts left-right locomotor coordination in mammalian spinal cord. Neuron, 60, 70–83. [PubMed: 18940589]

Deuchars SA (2105) How sympathetic are your spinal circuits? Exp Physiol, 100.4, 366–372.

Dougherty KJ & Kiehn O (2010) Functional organization of V2a-related locomotor circuits in the rodent spinal cord. Ann N Y Acad Sci, 1198, 85–93. [PubMed: 20536923]

Efron B & Tibshirani R (1991) Statistical data analysis in the computer age. Science, 253, 390–395. [PubMed: 17746394]

Fairless R, Frame MC & Barnett SC (2005) N-cadherin differentially determines Schwann cell and olfactory ensheathing cell adhesion and migration responses upon contact with astrocytes. Mol Cell Neurosci, 28, 253–263. [PubMed: 15691707]

Gad P, Choe J, Nandra MS, Zhong H, Roy RR, Tai YC & Edgerton VR (2013) Development of a multi-electrode array for spinal cord epidural stimulation to facilitate stepping and standing after a complete spinal cord injury in adult rats. J Neuroeng Rehabil, 10, 2. [PubMed: 23336733]

Gad P, Choe J, Nandra MS, Zhong H, Roy RR, Tai YC & Edgerton VR (2015) Erratum: development of a multi-electrode array for spinal cord epidural stimulation to facilitate stepping and standing after a complete spinal cord injury in adult rats. J Neuroeng Rehabil, 12, 33. [PubMed: 25889487]

Gerasimenko YP, Ichiyama RM, Lavrov IA, Courtine G, Cai L, Zhong H, Roy RR & Edgerton VR (2007) Epidural spinal cord stimulation plus quipazine administration enable stepping in complete spinal adult rats. J Neurophysiol, 98, 2525–2536. [PubMed: 17855582]

Guest JD, Herrera L, Margitich I, Oliveria M, Marcillo A & Casas CE (2008) Xenografts of expanded primate olfactory ensheathing glia support transient behavioral recovery that is independent of serotonergic or corticospinal axonal regeneration in nude rats following spinal cord transection. Exp Neurol, 212, 261–274. [PubMed: 18511045]

Author Manuscript Author Manuscript Author Manuscript Author Manuscript

Harkema S, Gerasimenko Y, Hodes J, Burdick J, Angeli C, Chen Y, Ferreira C, Willhite A, Rejc E, Grossman RG & Edgerton VR (2011) Effect of epidural stimulation of the lumbosacral spinal cord on voluntary movement, standing, and assisted stepping after motor complete paraplegia: a case study. Lancet, 377, 1938–1947. [PubMed: 21601270]

Huang A, Noga BR, Carr PA, Fedirchuk B, & Jordon LM (2000) Spinal cholinergic neurons activated during locomotion: Localization and electrophysiological characterization. J Neurophysiol, 83, 3537–3547. [PubMed: 10848569]

Ichiyama RM, Gerasimenko YP, Zhong H, Roy RR & Edgerton VR (2005) Hindlimb stepping movements in complete spinal rats induced by epidural spinal cord stimulation. Neurosci Lett, 383, 339–344. [PubMed: 15878636]

Iyer S, Maybhate A, Presacco A & All AH (2010) Multi-limb acquisition of motor evoked potentials and its application in spinal cord injury. J Neurosci Methods, 193, 210–216. [PubMed: 20832429]

Jordan LM, McVagh JR, Noga BR, Cabaj AM, Majczyński H, Sławińska U, Provencher J, Leblond H & Rossignol S (2014) Cholinergic mechanisms in spinal locomotion-potential target for rehabilitation approaches. Front Neural Circuits, 8, 132. [PubMed: 25414645]

Kasten MR, Sunshine MD, Secrist ES, Horner PJ & Moritz CT (2013) Therapeutic intraspinal microstimulation improves forelimb function after cervical contusion injury. J Neural Eng, 10, 044001. [PubMed: 23715242]

Kerman IA, Enquist LW, Watson SJ & Yates BJ (2003) Brainstem substrates of sympatho-motor circuitry identified using trans-synaptic tracing with pseudorabies virus recombinants. J Neurosci, 23, 4657–4666. [PubMed: 12805305]

Keyvan-Fouladi N, Raisman G & Li Y (2003) Functional repair of the corticospinal tract by delayed transplantation of olfactory ensheathing cells in adult rats. J Neurosci, 23, 9428–9434. [PubMed: 14561871]

Khankan RR, Griffis KG, Haggerty-Skeans JR, Zhong H, Roy RR, Edgerton VR & Phelps PE (2016) Olfactory ensheathing cell transplantation after a complete spinal cord transection mediates neuroprotective and immunomodulatory mechanisms to facilitate regeneration. J Neurosci, 36, 6269–6286. [PubMed: 27277804]

Khankan RR, Wanner IB & Phelps PE (2015) Olfactory ensheathing cell-neurite alignment enhances neurite outgrowth in scar-like cultures. Exp Neurol, 269, 93–101. [PubMed: 25863021]

Kubasak MD, Jindrich DL, Zhong H, Takeoka A, McFarland KC, Muñoz-Quiles C, Roy RR, Edgerton VR, Ramón-Cueto A & Phelps PE (2008) OEG implantation and step training enhance hindlimb-stepping ability in adult spinal transected rats. Brain, 131, 264–276. [PubMed: 18056162]

Lakatos A, Barnett SC & Franklin RJ (2003) Olfactory ensheathing cells induce less host astrocyte response and chondroitin sulphate proteoglycan expression than Schwann cells following transplantation into adult CNS white matter. Exp Neurol, 184, 237–246. [PubMed: 14637095]

Lakatos A, Franklin RJ & Barnett SC (2000) Olfactory ensheathing cells and Schwann cells differ in their in vitro interactions with astrocytes. Glia, 32, 214–225. [PubMed: 11102963]

Lavrov I, Dy CJ, Fong AJ, Gerasimenko Y, Courtine G, Zhong H, Roy RR & Edgerton VR (2008) Epidural stimulation induced modulation of spinal locomotor networks in adult spinal rats. J Neurosci, 28, 6022–6029. [PubMed: 18524907]

Lavrov I, Gerasimenko YP, Ichiyama RM, Courtine G, Zhong H, Roy RR & Edgerton VR (2006) Plasticity of spinal cord reflexes after a complete transection in adult rats: relationship to stepping ability. J Neurophysiol, 96, 1699–1710. [PubMed: 16823028]

Li Y, Field PM & Raisman G (1997) Repair of adult rat corticospinal tract by transplants of olfactory ensheathing cells. Science, 277, 2000–2002. [PubMed: 9302296]

Li Y, Li D & Raisman G (2005) Interaction of olfactory ensheathing cells with astrocytes may be the key to repair of tract injuries in the spinal cord: the ‘pathway hypothesis’. J Neurocytol, 34, 343–351. [PubMed: 16841171]

Li Y, Li D & Raisman G (2016) Functional repair of rat corticospinal tract lesions does not require permanent survival of an immunoincompatible transplant. Cell Transplant, 25, 293–299. [PubMed: 26132822]

Lipson AC, Widenfalk J, Lindqvist E, Ebendal T & Olson L (2003) Neurotrophic properties of olfactory ensheathing glia. Exp Neurol, 180, 167–171. [PubMed: 12684030]

Author Manuscript Author Manuscript Author Manuscript Author Manuscript

López-Vales R, Forés J, Navarro X & Verdú E (2007) Chronic transplantation of olfactory ensheathing cells promotes partial recovery after complete spinal cord transection in the rat. Glia, 55, 303–311. [PubMed: 17096411]

Mennerick S & Zorumski CF (2000) Neural activity and survival in the developing nervous system. Mol Neurobiol, 22, 41–54. [PubMed: 11414280]

Miles GB, Hartley R, Todd AJ & Brownstone RM (2007) Spinal cholinergic interneurons regulate the excitability of motoneurons during locomotion. Proc Natl Acad Sci U S A, 104, 2448–2453. [PubMed: 17287343]

Mondello SE, Kasten MR, Horner PJ & Moritz CT (2014) Therapeutic intraspinal stimulation to generate activity and promote long-term recovery. Front Neurosci, 8, 21. [PubMed: 24578680]

Ni Y, Nawabi H, Liu X, Yang L, Miyamichi K, Tedeschi A, Xu B, Wall NR, Callaway EM & He Z (2014) Characterization of long descending premotor propriospinal neurons in the spinal cord. J Neurosci, 34, 9404–9417. [PubMed: 25009272]

Perry AC, Wakayama T, Kishikawa H, Kasai T, Okabe M, Toyoda Y & Yanagimachi R (1999) Mammalian transgenesis by intracytoplasmic sperm injection. Science, 284, 1180–1183. [PubMed: 10325231]

Phelps PE, Barber RP, Houser CR, Crawford GD, Salvaterra PM & Vaughn JE (1984) Postnatal development of neurons containing choline acetyltransferase in rat spinal cord: an immunocytochemical study. J Comp Neurol, 229, 347–361. [PubMed: 6389614]

Phelps PE, Brennan LA, Vaughn JE (1990) Generation patterns of immunocytochemically identified cholinergic neurons in rat brainstem. Dev Brain Res, 56, 63–74. [PubMed: 2279332]

Plant GW, Christensen CL, Oudega M & Bunge MB (2003) Delayed transplantation of olfactory ensheathing glia promotes sparing/regeneration of supraspinal axons in the contused adult rat spinal cord. J Neurotrauma, 20, 1–16. [PubMed: 12614584]

Ramón-Cueto A, Cordero MI, Santos-Benito FF & Avila J (2000) Functional recovery of paraplegic rats and motor axon regeneration in their spinal cords by olfactory ensheathing glia. Neuron, 25, 425–435. [PubMed: 10719896]

Ramón-Cueto A, Plant GW, Avila J & Bunge MB (1998) Long-distance axonal regeneration in the transected adult rat spinal cord is promoted by olfactory ensheathing glia transplants. J Neurosci, 18, 3803–3815. [PubMed: 9570810]

Rejc E, Angeli C & Harkema S (2015) Effects of lumbosacral spinal cord epidural stimulation for standing after chronic complete paralysis in humans. PLoS One, 10, e0133998. [PubMed: 26207623]

Rotto-Percelay DM, Wheeler JG, Osorio FA, Platt KB & Loewy AD (1992) Transneuronal labeling of spinal interneurons and sympathetic preganglionic neurons after pseudorabies virus injections in the rat medial gastrocnemius muscle. Brain Res, 574, 291–306. [PubMed: 1322222]

Roy RR, Hodgson JA, Lauretz SD, Pierotti DJ, Gayek RJ & Edgerton VR (1992) Chronic spinal cord-injured cats: surgical procedures and management. Lab Anim Sci, 42, 335–343. [PubMed: 1434492]

Runyan SA & Phelps PE (2009) Mouse olfactory ensheathing glia enhance axon outgrowth on a myelin substrate in vitro. Exp Neurol, 216, 95–104. [PubMed: 19100263]

Schramm LP (2006) Spinal sympathetic interneurons: Their identification and roles after spinal cord injury, in: Weaver LC, Polosa C (Eds), Progress in Brain Research, Vol. 152, Elsevier B.V., pp. 27–37.

Steward O, Zheng B & Tessier-Lavigne M (2003) False resurrections: distinguishing regenerated from spared axons in the injured central nervous system. J Comp Neurol, 459, 1–8. [PubMed: 12629662]

Tabakow P, Raisman G, Fortuna W, Czyz M, Huber J, Li D, Szewczyk P, Okurowski S, Miedzybrodzki R, Czapiga B, Salomon B, Halon A, Li Y, Lipiec J, Kulczyk A & Jarmundowicz W (2014) Functional regeneration of supraspinal connections in a patient with transected spinal cord following transplantation of bulbar olfactory ensheathing cells with peripheral nerve bridging. Cell Transplant, 23, 1631–1655. [PubMed: 25338642]

Takashima A (2001) Establishment of fibroblast cultures, in: Current Protocol Cell Biology. Wiley, Hoboken, NJ, pp. Unit 2.1.1–2.1.12.

Author Manuscript Author Manuscript Author Manuscript Author Manuscript

Takeoka A, Jindrich DL, Muñoz-Quiles C, Zhong H, van den Brand R, Pham DL, Ziegler MD, Ramón-Cueto A, Roy RR, Edgerton VR & Phelps PE (2011) Axon regeneration can facilitate or suppress hindlimb function after olfactory ensheathing glia transplantation. J Neurosci, 31, 4298–4310. [PubMed: 21411671]

Tetzlaff W, Okon EB, Karimi-Abdolrezaee S, Hill CE, Sparling JS, Plemel JR, Plunet WT, Tsai EC, Baptiste D, Smithson LJ, Kawaja MD, Fehlings MG & Kwon BK (2011) A systematic review of cellular transplantation therapies for spinal cord injury. J Neurotrauma, 28, 1611–1682. [PubMed: 20146557]

Tillakaratne NJ, Duru P, Fujino H, Zhong H, Xiao MS, Edgerton VR & Roy RR (2014) Identification of interneurons activated at different inclines during treadmill locomotion in adult rats. J Neurosci Res, 92, 1714–1722. [PubMed: 24975393]

Ueno M, Nakamura Y, Li J, Gu Z, Niehaus J, Maezawa M. Crone SA, Goulding M, Baccei ML, Yoshida Y (2018) Corticospinal circuits from the sensory and motor cortices differentially regulate skilled movements through distinct spinal interneurons. Cell Reports, 23, 1286–1300. [PubMed: 29719245]

Ueno M, Ueno-Nakamura Y, Niehaus J, Popovich PG, Yoshida Y (2016) Silencing spinal interneurons inhibits immune suppressive autonomic reflexes caused by spinal cord injury. Nat Neurosci, 19, 784–787. [PubMed: 27089020]

Watzlawick R, Rind J, Sena ES, Brommer B, Zhang T, Kopp MA, Dirnagl U, Macleod MR, Howells DW & Schwab JM (2016) Olfactory ensheathing cell transplantation in experimental spinal cord injury: Effect size and reporting bias of 62 experimental treatments: A systematic review and meta-analysis. PLoS Biol, 14, e1002468. [PubMed: 27244556]

Woodhall E, West AK & Chuah MI (2001) Cultured olfactory ensheathing cells express nerve growth factor, brain-derived neurotrophic factor, glia cell line-derived neurotrophic factor and their receptors. Brain Res Mol Brain Res, 88, 203–213. [PubMed: 11295250]

Zagoraiou L, Akay T, Martin JF, Brownstone RM, Jessell TM, & Miles GB, (2009) A cluster of cholinergie premotor interneurons modulate mouse locomotor activity. Neuron, 64, 645–662. [PubMed: 20005822]

Zholudeva LV, Karliner JS, Dougherty KJ, & Lane MA (2017) Anatomical recruitment of spinal V2a interneurons into phrenic motor circuitry after high cervical spinal cord injury. J Neurotrauma, 34, 3058–3065. [PubMed: 28548606]

Ziegler MD, Hsu D, Takeoka A, Zhong H, Ramón-Cueto A, Phelps PE, Roy RR & Edgerton VR (2011) Further evidence of olfactory ensheathing glia facilitating axonal regeneration after a complete spinal cord transection. Exp Neurol, 229, 109–119. [PubMed: 21272578]

Author Manuscript Author Manuscript Author Manuscript Author Manuscript

HIGHLIGHTS

- When combined with long-term epidural stimulation and climb training, olfactory ensheathing cell (OEC) transplantation facilitated serotonergic- and neurofilament-labeled axon projections into the injury site of rats following severe spinal cord transection.
- Two of ten rats had clear axonal connectivity across the transection site. The OEC-treated rat had apparent evidence of axon regeneration while the FB-treated rat had a small area of axon sparing.
- After pseudorabies virus injections into hindlimb muscles, two spinal rats had labeled V2a propriospinal interneurons within and rostral to the transection site.

Author Manuscript Author Manuscript Author Manuscript Author Manuscript

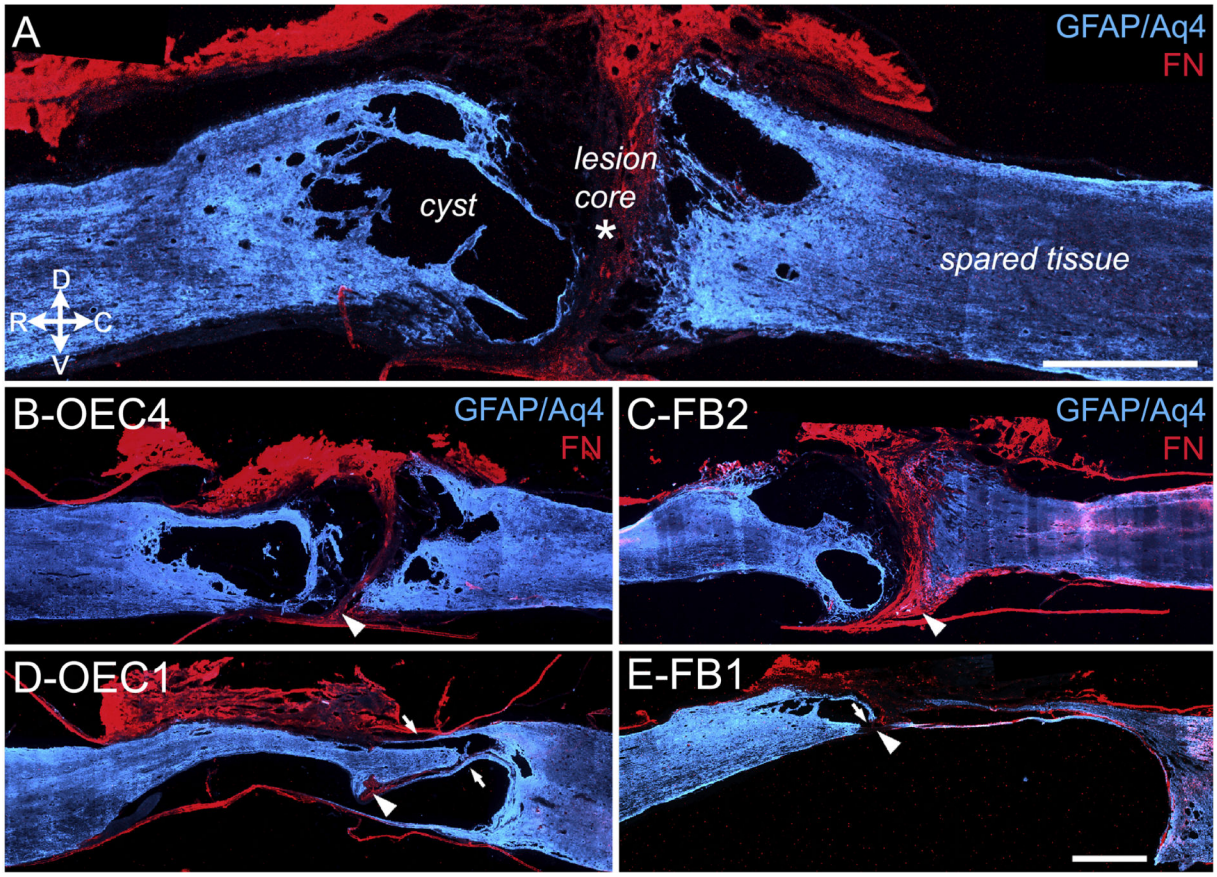

Figure 1: Structural analyses of injury sites at 7-months post-transection.

Astrocytes (GFAP plus Aquaporin-4, Aq-4, blue) and the fibrotic extracellular matrix of the lesion core (Fibronectin, FN, red) were identified in sagittal sections of the injury site. **A**, The complete transection site is marked by a FN-positive lesion core (asterisk) between the spinal stumps, and spared GFAP-positive tissue (blue) that also surrounds several cysts. Note the relative size of the spinal cysts ('secondary injury') to the FN-positive lesion core ('primary injury') in this severe SCI model. **B**, **C**, Representative sections from OEC-transplanted rat #4 (B) and FB-transplanted rat #2 (C) show a clear separation of the rostral and caudal spinal stumps at the FN-immunoreactive lesion core (arrowheads). **D**, **E**, OEC rat #1 (D) and FB rat #1 (E) have nearly continuous GFAP immunoreactivity that extends across the lesion core and connects the spinal stumps. Arrowheads denote the small FN-rich areas that may represent the initial transection sites. Arrows mark thin GFAP-positive astrocyte extensions and possible bridges. Rostral is toward the left and dorsal toward the top in these and subsequent sagittal sections. Scale bars in A, B-E = 1000 μm.

Author Manuscript Author Manuscript Author Manuscript Author Manuscript

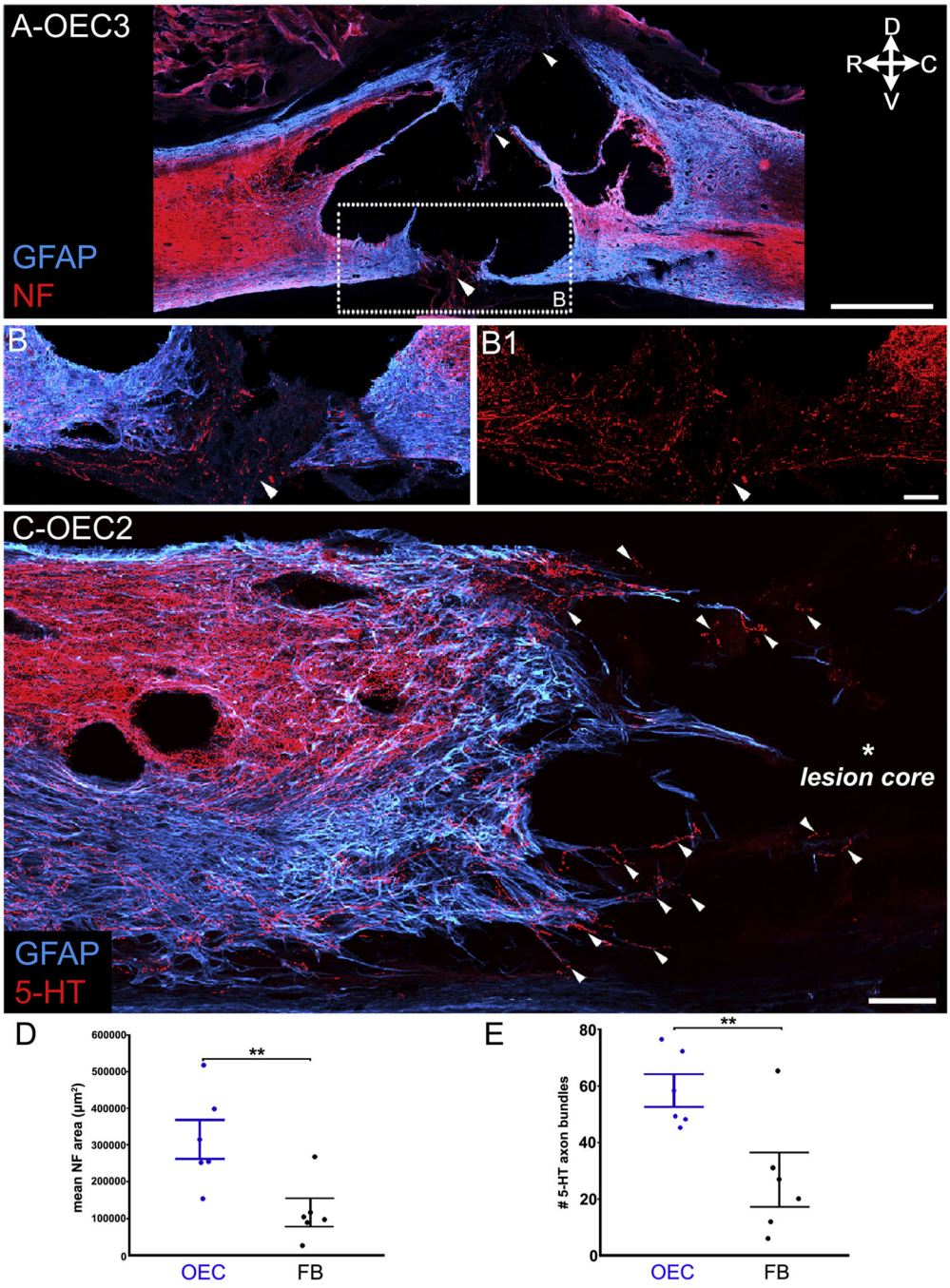

Figure 2: OEC-injected rats had greater areas of NF in the injury site and more 5-HT axon bundles that crossed the rostral scar border than FB-injected rats.

Sagittal sections of the injury sites show astrocytes (A–C, GFAP, blue) and neurofilament (A, B–B1, NF, red) or serotonergic-labeled (C, 5-HT, red) axons. **A**, Injury site from OEC #3 has multiple areas with possible continuity of GFAP and NF (white arrowheads). **B**, **B1**, A confocal image of the ventral bridge boxed in A was imaged from a section ~400 μm medial to A. NF-positive axons (white arrowheads) were detected in the GFAP-negative region between the rostral and caudal stumps. **C**, The rostral scar border of OEC #2 shows

Author Manuscript Author Manuscript Author Manuscript Author Manuscript

multiple extensions of GFAP-labeled astrocytes with many 5-HT-positive axons (white arrowheads) that project into the lesion core. **D**, OEC-transplanted rats had greater areas of NF immunoreactivity in the injury site than FB-treated rats (**$p = 0.002$). **E**, OEC-transplanted rats had more 5-HT axon bundles that crossed the rostral scar border than the FB-transplanted rats (**$p = 0.007$). Dot plots show the mean value for each rat and group mean +/− SEM in this and the subsequent figure. Confocal images (A–C) are collapsed z-stack projections, 12–15 μm thick. Scale bars: A = 1000 μm, B–B1, C= 100 μm.

Author Manuscript Author Manuscript Author Manuscript Author Manuscript

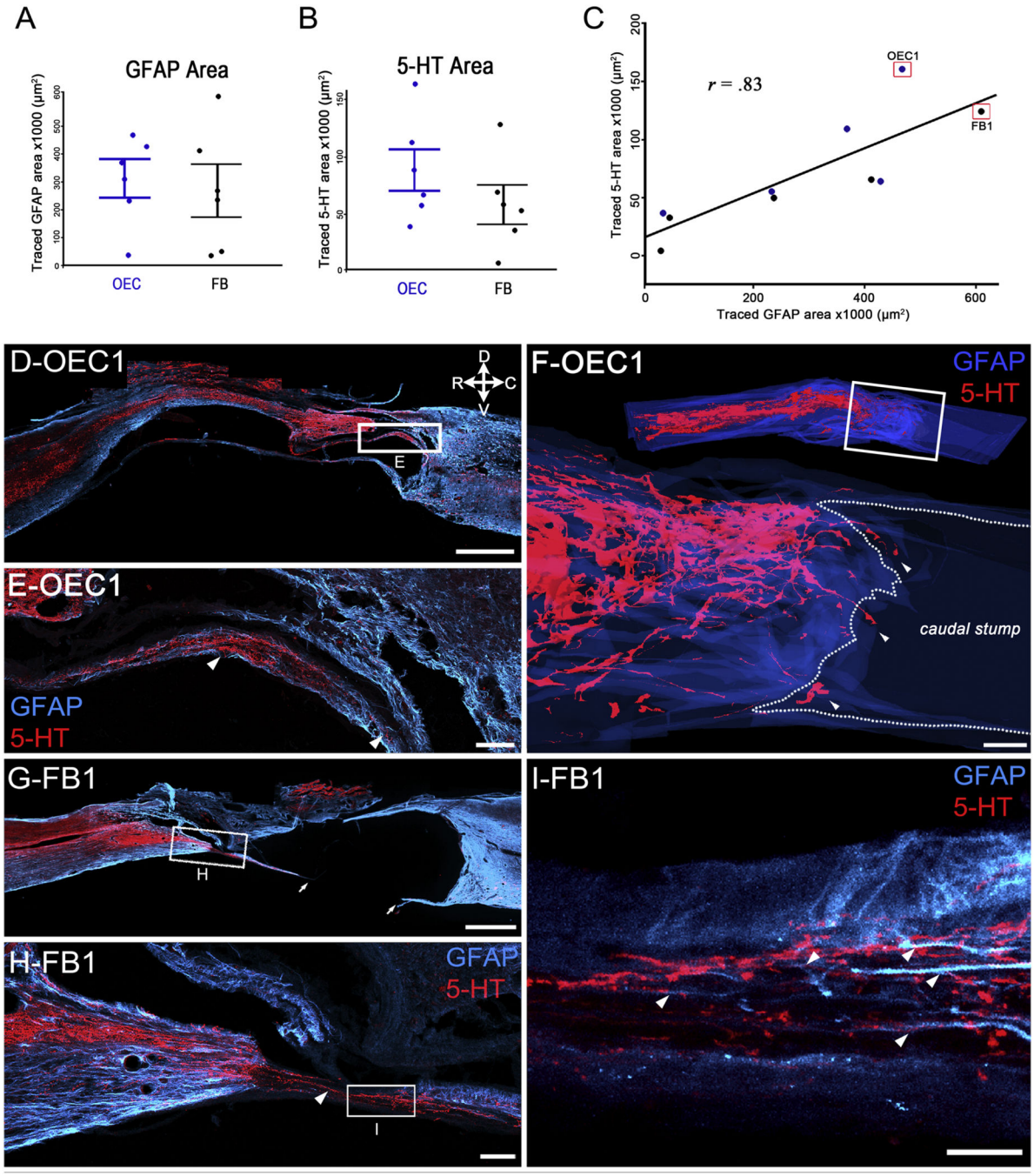

Figure 3: Serotonergic axons extended through the lesion core on thin astrocyte bridges.

Sagittal sections of injury sites were labeled for astrocytes (GFAP, blue) and serotonergic axons (5-HT, red). **A-C**, The areas of GFAP-positive astrocyte extensions (A) and the 5-HT-positive axon area (B) in the injury site did not differ between OEC- and FB-treated rats. When the GFAP and 5-HT measures were plotted together (C) a strong positive correlation between the two was evident ($r = .83$, $^{**}p = 0.003$). Data points boxed in red represent the 2 rats illustrated in D–I. **D–E**, OEC rat #1 has a thin astrocytic bridge that connects the rostral and caudal stumps and is associated with bundles of 5-HT axons (D). The box in D is

Author Manuscript Author Manuscript Author Manuscript Author Manuscript

enlarged in E and shows 5-HT axons (white arrowheads) that extend toward the caudal stump. **F**, The top image is a sagittal view of a 3-D spinal cord reconstruction of the injury site of OEC #1 and the white box in D orients the area of the 3-D reconstruction of 5-HT axon bundles (white arrowheads) that project through the injury site and into the caudal stump (bottom image). The caudal stump is outlined (dotted line) and appears dark blue. A rotating animation of the 3-D reconstruction is provided as Supplemental Video 1. **G–I**, The boxed area of the injury site of FB #1 in G is enlarged in H and shows a bridge that contains 5-HT axons (H, white arrowhead). I is a higher magnification of the boxed area in H and depicts elongated astrocytic processes (white arrowheads) that are associated with red 5-HT-positive axons. Arrows in G show an area that was likely connected but damaged during tissue processing. Confocal images (E, H, I) are collapsed ~15 μm thick z-stack projections. Scale bars: D, F, G = 1000 μm, E, H = 100 μm, I = 20 μm.

Author Manuscript
Author Manuscript
Author Manuscript
Author Manuscript

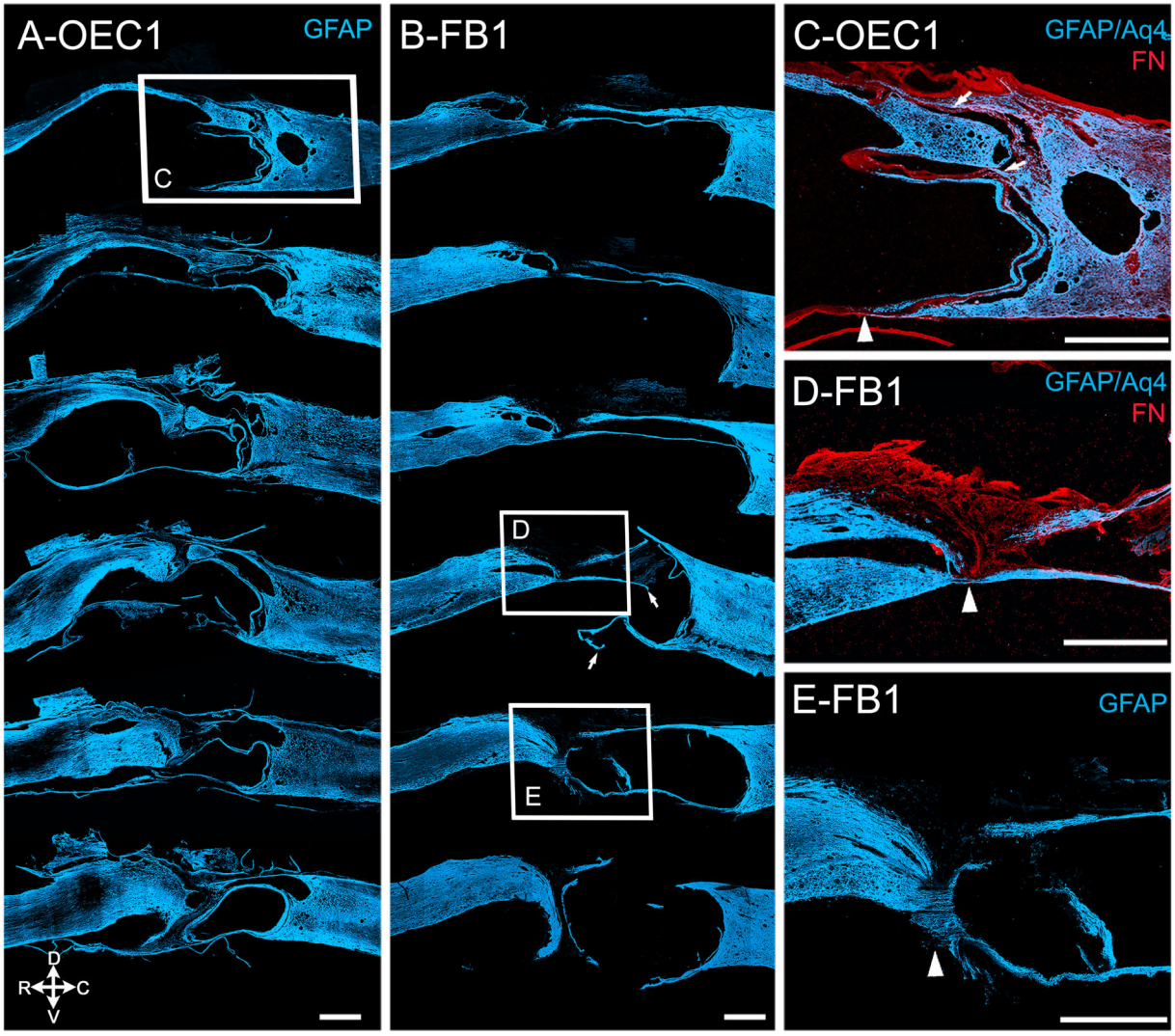

Figure 4: The glial bridges in the injury sites of OEC #1 and FB #1 differ along the dorso-ventral axis.

Sagittal injury site sections of two spinal rats show the astrocytic scar border (A-E, GFAP, blue) and the lesion core (C, D, fibronectin, red). **A**, **B**, Six representative injury site sections from OEC-treated rat #1 (A) and FB-treated rat #1 (B) are spaced at 200–400 μm intervals. Arrows (B) indicate areas that were likely connected but damaged during tissue processing. **C**, Enlargement of the boxed area in A. The GFAP-labeled ventral glial scar aligns with the FN-positive scar (red, arrowhead). Despite the discontinuity of the ventral spinal cord, dorsal and intermediate astrocyte bridges (arrows) are present. **D**, **E**, Enlargements of boxes D and E from B show a continuous glial bridge on the ventral surface of the injury site (arrowheads) in FB #1. Note that in D the fibrotic lesion core (FN, red) separates all except the ventral spinal stumps. A distinct piece of ventral tissue connects the two stumps in E (arrowhead). The intact ventral bridge continues at least 200 μm between sections D and E. Scale bars in A-E = 1000 μm.

Author Manuscript Author Manuscript Author Manuscript Author Manuscript

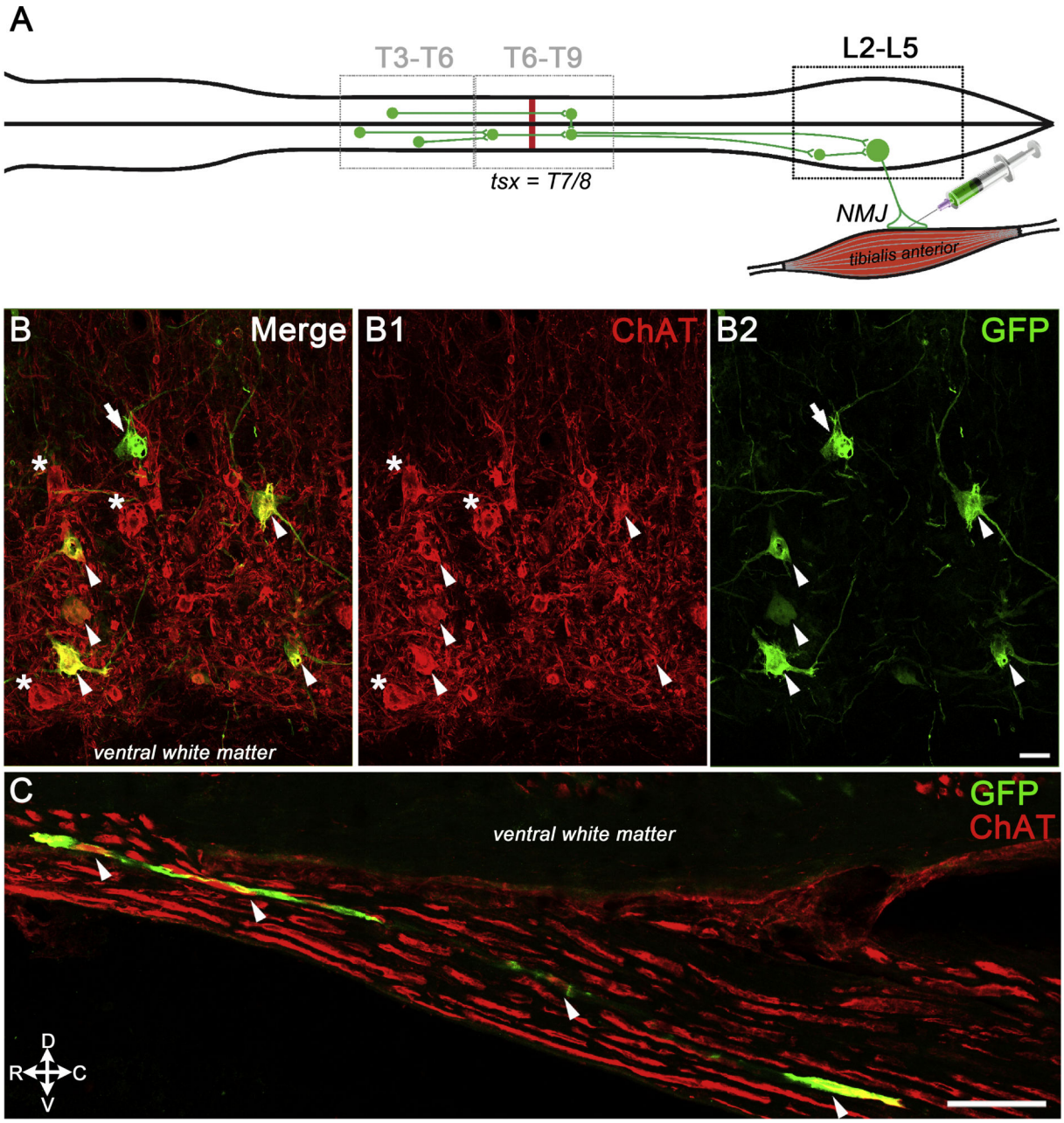

Figure 5: PRV injections into the tibialis anterior identified lumbar somatic motor neurons (SMNs).

A, Schematic shows an example of the retrograde infection of lumbar SMNs from the tibialis anterior neuromuscular junctions and the subsequent infection of both ipsilateral and contralateral interneurons in the lumbar and thoracic spinal cord. The T7/T8 spinal cord transection is represented with a red line. **B-B2**, Confocal images of multiple ventral neurons co-express GFP (B, B2) and ChAT (B, B1, white arrowheads), and confirm the viral infection of lumbar SMNs. One large PRVeGFP-positive neuron does not express ChAT (B, B2, white arrow) and several ChAT-positive SMNs are not labeled with PRV (B, B1, white asterisks). **C**, PRVeGFP and ChAT-labeled axon bundles (white arrowheads) are detected in

the L4/L5 ventral root and illustrate the viral entry route into the lumbar spinal cord. Scale bars B–B2, C = 50 μm.

Author Manuscript Author Manuscript Author Manuscript Author Manuscript

Author Manuscript Author Manuscript Author Manuscript Author Manuscript

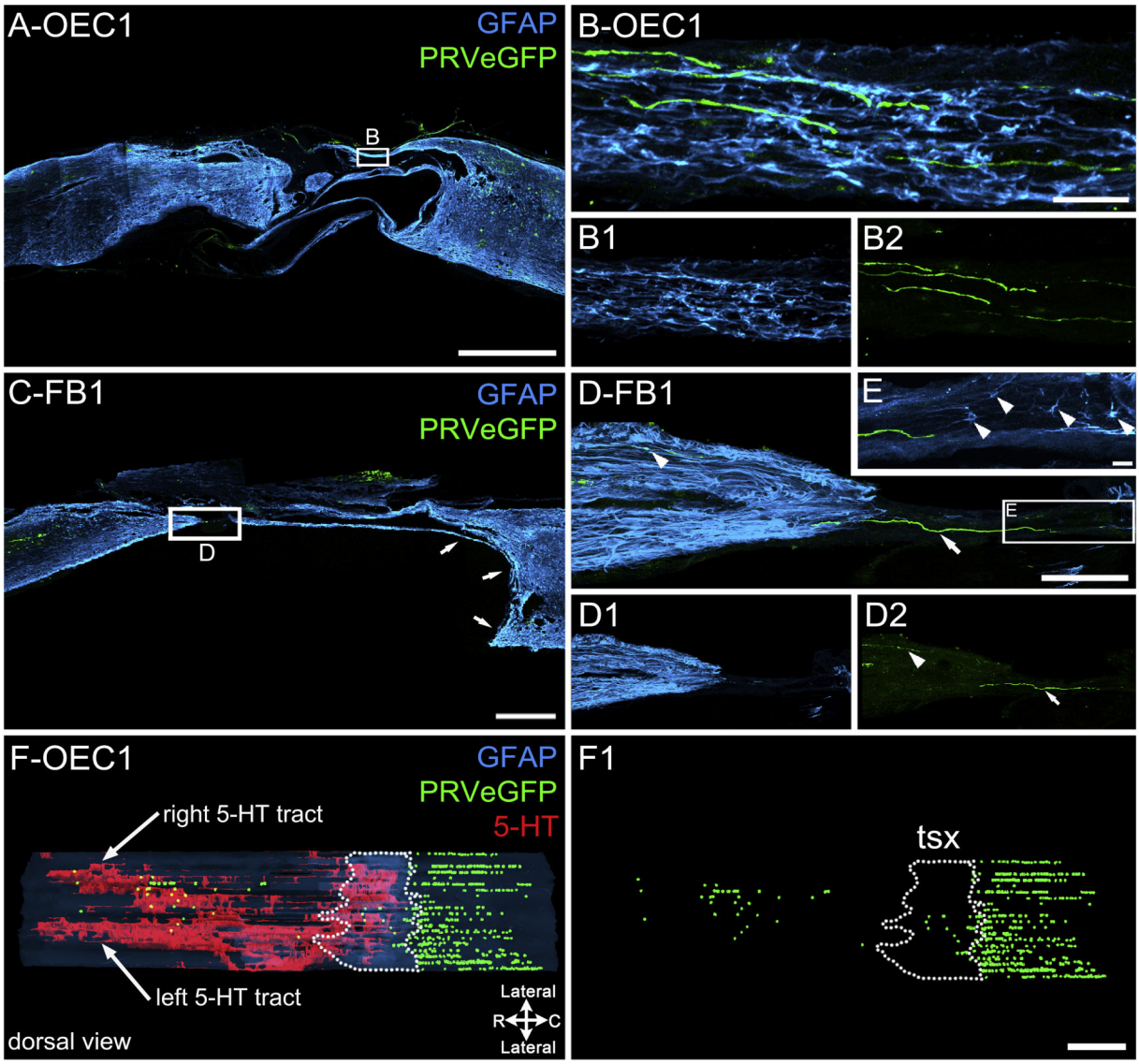

Figure 6: PRV-labeled axons are detected in the injury site of two spinal rats.

Injury sites are labeled for astrocytes (GFAP, blue) and PRVeGFP-infected neurons (green). **A**, Sagittal injury site section from OEC #1 has multiple GFAP-labeled extensions between the rostral and caudal stumps. **B–B2**, Enlargement of a small box in A shows possible astrocyte bridges (B, B1, blue) that are associated with PRV-labeled axons (B, B2, green) within the injury site. **C**, Sagittal injury site section from FB #1 has a single GFAP-labeled extension (small arrows) that likely surrounded a large, ventrally located cyst in the caudal stump. **D–D2**, Enlargement of boxed area in C shows a green PRVeGFP-labeled axon that coursed between the rostral and the caudal stumps (white arrow) and a smaller axon within the rostral stump (white arrowhead). **E**, Enlargement of boxed area in D shows several astrocytes (white arrowheads) associated with the caudal side of the axon bridge. **F, F1**, A dorsal view of the full 3-D spinal cord reconstruction for OEC #1 shows the spatial relationship between descending 5-HT axon tracts (red), PRVeGFP-labeled cell bodies (green spheres), and the estimated injury site (area enclosed by dotted line). In F1, only

Author Manuscript Author Manuscript Author Manuscript Author Manuscript

PRVeGFP-labeled neurons are shown relative to the estimated transection site (tsx, dotted line). Note that many PRVeGFP-labeled cells were found within and rostral to the injury site. Scale bars A, C, F–F1 = 1000 μm, B–B2, E = 20 μm, D–D2 = 200 μm.

Author Manuscript Author Manuscript Author Manuscript Author Manuscript

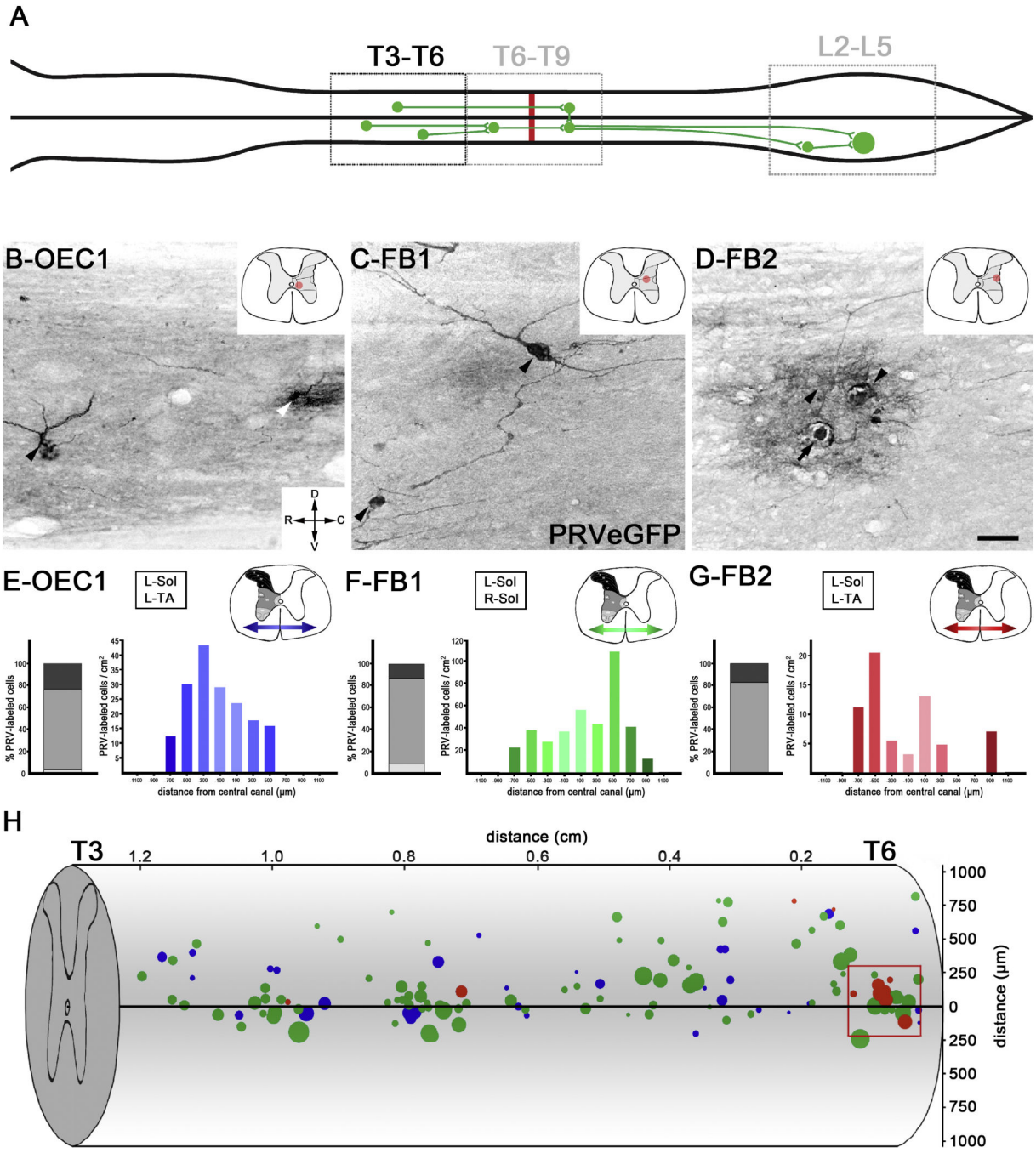

Figure 7: PRV labeling was detected in thoracic neurons rostral to the injury site.

A, Schematic of retrograde PRV transport to thoracic neurons rostral to the T7/T8 transection (red line). **B-D**, PRVeGFP-labeled cells rostral to the injury site were found in 3/8 rats with PRV-infected lumbar SMNs (OEC #1, FB #1, FB #2). Images show representative cells from each rat and the red dot on the transverse section sketch (upper right corner) marks the estimated location of the cells. Two PRVeGFP-labeled neurons from the thoracic intermediate grey matter of OEC #1 are shown (B) but the neuron on the right (white arrowhead) may have been lysed due to the PRV infection. Two PRVeGFP-labeled

Author Manuscript Author Manuscript Author Manuscript Author Manuscript

neurons found in FB #1 (C, black arrowheads), one of which has extensive processes in the intermediate grey matter. In FB #2, a cluster of PRVeGFP-labeled neurons (D, arrowheads) was detected in the intermediolateral grey matter (D). One labeled cell has a ruptured somata (black arrow) and the reaction product surrounding the nuclei indicates post-infection lysis and likely reactive astrogliosis. **E-G**, Locations of PRVeGFP-labeled cells were determined throughout the T3–T6 spinal cord segments for these 3 rats. Cells were grouped in three bins along the dorsoventral axis (shown on the schematic in the upper right corner, greyscale) and the percent of cells in each bin is reported in a stacked bar graph (left for each image). Cells were also binned along the mediolateral axis (two directional arrows on each schematic) and reported as cell counts/cm^2 in a histogram plot (note y-axis scales vary). Muscles injected with PRVeGFP listed for each rat. **H**, The rostrocaudal (x-axis) and dorsoventral (y-axis) distribution of PRVeGFP-labeled cells were mapped in the T3–T6 segments for OEC #1 (blue), FB #1 (green), and FB #2 (red) and overlaid onto a spinal cord drawing. The size of the dots represents the long axis of each cell body. The red box contains a cluster of lateral spinal neurons near the intermediolateral cell column of FB #2. Scale bars B-D = 50 μm.

Author Manuscript Author Manuscript Author Manuscript Author Manuscript

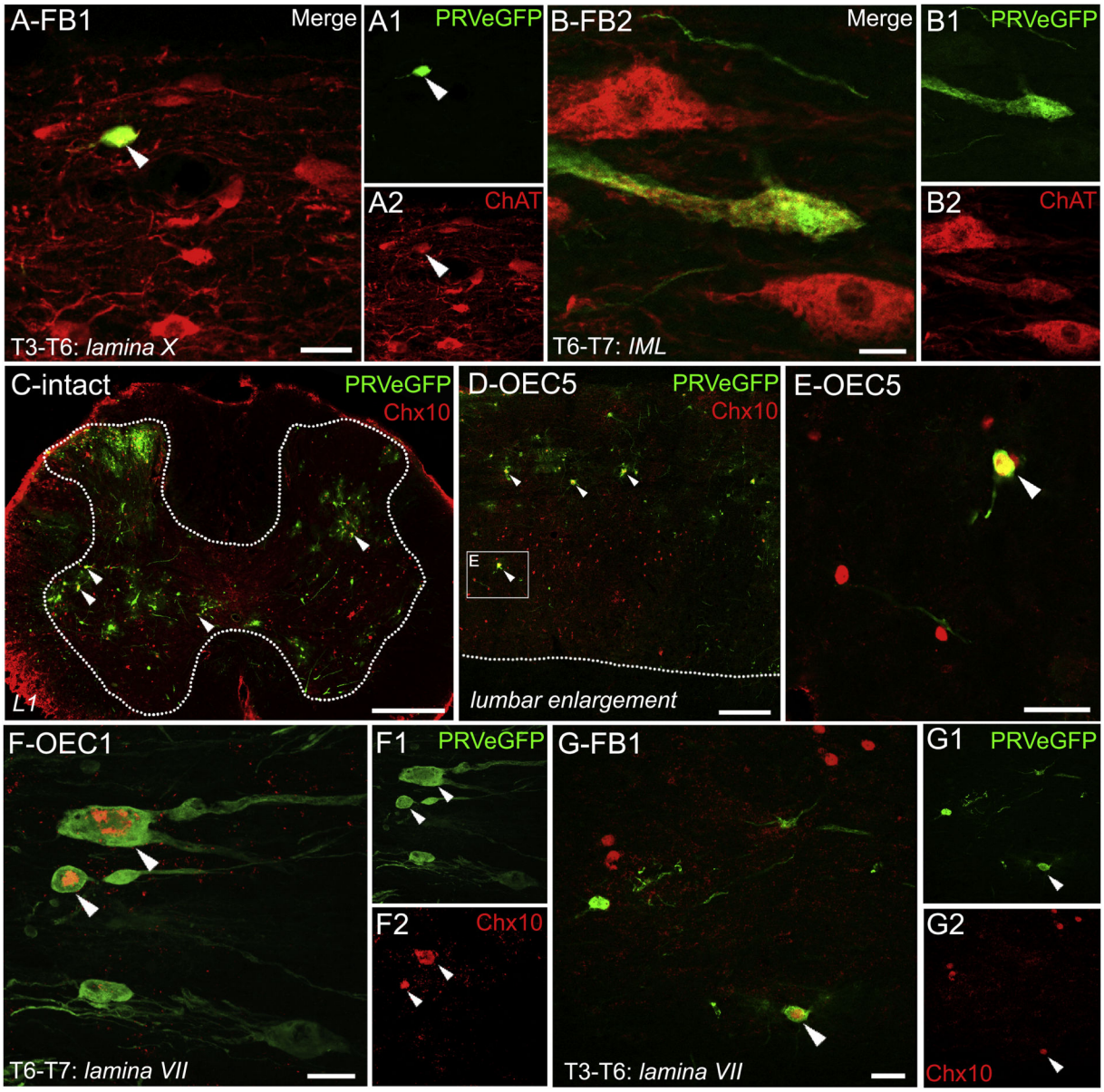

Figure 8: Cholinergic and V2a interneurons were infected with PRV rostral to the spinal cord transection.

PRVeGFP-infected neurons (A–G, green), cholinergic neurons (A–B, red), and Chx10-positive nuclei (C–G, red). **A–A2**, Confocal images of a PRVeGFP-positive cell (A, A1) that co-localizes with ChAT (A, A2, white arrowheads) in a midline sagittal section near lamina X in the T3–T6 region of FB #1. **B–B2**, A large cholinergic neuron from a lateral section from the T6–T7 region of FB #2 (B, B2) co-localizes with PRVeGFP (B, B1) in the IML cell column. **C**, Chx10 marks V2a interneurons and is expressed in an upper lumbar transverse section of an intact adult rat injected with PRV. Multiple Chx10-positive interneurons co-localize (white arrowheads) with the PRV. White dotted lines mark the spinal grey-white matter interface in C and D. **D, E**, A sagittal section from the lumbar enlargement of OEC #5 shows a pattern of Chx10 expression similar to that of the intact rat (C). Enlargement of

Author Manuscript Author Manuscript Author Manuscript Author Manuscript

the box in D shows a V2a interneuron colocalized with PRVeGFP and Chx10 (E, white arrowhead) that is directly adjacent to a second, uninfected Chx10-positive nucleus. Several uninfected Chx10-positive nuclei are nearby. **F–F2**, Two V2a interneurons co-express PRVeGFP and Chx10 (F1, F2, arrowheads) and were detected rostral to the injury site in OEC #1, the rat with strong evidence of axon regeneration. **G–G2**, A V2a interneuron that co-expresses PRVeGFP and Chx10 (G1, G2, arrowheads) was found rostral to the transection in FB #1, the rat with spared axons that crossed the injury site. Confocal images (A, B, F, G) are single slices. Scale bars: A, B, F, and G = 20 μm, C= 400 μm, D = 200 μm, and E = 50 μm.